AFRL-SR-AR-TR-09-0129

REPORT DOCUMENTATION PAGE

1. REPORT DATE *(DD-MM-YYYY)*	2. REPORT TYPE	3. DATES COVERED *(From - To)*
25-02-2009	Final	May 2007 - December 2008

4. TITLE AND SUBTITLE
Analysis of Plasma Communication Schemes for Hypersonic Vehicles: Final Report

5a. CONTRACT NUMBER
FA9550-07-C-0049

5b. GRANT NUMBER

5c. PROGRAM ELEMENT NUMBER

6. AUTHOR(S)
Rose, David V., Voss Scientific, LLC
Thoma, Carsten H., Voss Scientific, LLC
Sotnikov, Vladimir, University of Nevada, Reno

5d. PROJECT NUMBER

5e. TASK NUMBER

5f. WORK UNIT NUMBER

7. PERFORMING ORGANIZATION NAME(S) AND ADDRESS(ES)
Voss Scientific, LLC
418 Washington Street SE
Albuquerque NM 87108

8. PERFORMING ORGANIZATION REPORT NUMBER
VSL-0832

9. SPONSORING/MONITORING AGENCY NAME(S) AND ADDRESS(ES)
Air Force Office of Scientific Research/NE
875 North Randolph Street
Suite 325, Room 3112
Arlington VA 22203

10. SPONSOR/MONITOR'S ACRONYM(S)
AFOSR

11. SPONSOR/MONITOR'S REPORT NUMBER(S)

12. DISTRIBUTION/AVAILABILITY STATEMENT
Distribution Statement A. Approved for public release; distribution unlimited.

13. SUPPLEMENTARY NOTES

14. ABSTRACT

We summarize progress in our analysis of proposed communication schemes for hypersonic vehicles in flight. Investigations into the electron-acoustic wave (EAW) communication scheme have yielded a dispersion analysis indicating that EAW modes can be generated and propagate in the plasma layer. Furthermore, we have demonstrated that these modes can be coupled to EM waves at the plasma layer boundary for the assumption of a sharp density boundary. We discuss results of 1D particle-in-cell simulations of a plasma-filled cross-field diode. These simulations are intended to model some of the critical physical processes of the ReComm scheme for communications through the plasma sheath surrounding a hypersonic vehicle during re-entry. We demonstrate that the time required to significantly alter the plasma density profile in the diode corresponds roughly to the ambipolar diffusion time. When a voltage is applied, the plasma center-of-mass shifts from the center of the diode. But whether that shift is towards the cathode or anode depends sensitively on the relative mobility of the plasma ions and electrons.

15. SUBJECT TERMS
hypersonic vehicle communication, numerical simulations, electromagnetic wave propagation and attenuation, communication blackout

16. SECURITY CLASSIFICATION OF:			17. LIMITATION OF ABSTRACT	18. NUMBER OF PAGES	19a. NAME OF RESPONSIBLE PERSON
a. REPORT	b. ABSTRACT	c. THIS PAGE			David V. Rose
U	U	U	UU	1	19b. TELEPHONE NUMBER *(Include area code)* (505) 255-4201

VSL-0832

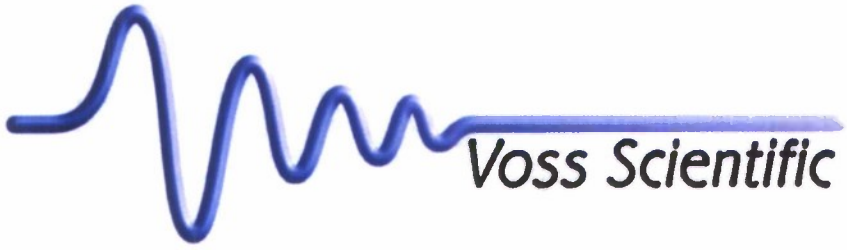

Analysis of Plasma Communication Schemes for Hypersonic Vehicles: Final Report

D. V. Rose, C. Thoma, and V. Sotnikov

February 2009

Prepared for: AFOSR/NE (Dr. Arje Nachman)
875 North Randolph Street
Ste 325, Room 3112
Arlington, VA 22203

Under Contract: FA9550-07-C-0049
CLIN 0002AC: Final Report

Prepared by: Voss Scientific, LLC
418 Washington, SE
Albuquerque, NM 87108
www.vosssci.com
(505) 255-4201

Abstract

We summarize progress in our analysis of proposed communication schemes for hypersonic vehicles in flight. Investigations into the electron-acoustic wave (EAW) communication scheme have yielded a dispersion analysis indicating that EAW modes can be generated and propagate in the plasma layer. Furthermore, we have demonstrated that these modes can be coupled to electromagnetic waves at the plasma layer boundary for the assumption of a sharp density boundary. A detailed analysis of the wave transformation coefficients at this boundary layer is presented. We also discuss the results of 1D particle-in-cell simulations of a plasma-filled cross-field diode. These simulations are intended to model some of the critical physical processes of the ReComm scheme for communications through the plasma sheath surrounding a hypersonic vehicle during re-entry. The ReComm scheme utilizes externally generated crossed electric and magnetic fields to induce charged-particle drifts. This spatially redistributes the plasma and enables propagation of electromagnetic waves through the plasma layer. We demonstrate that the time required to significantly alter the plasma density profile in the diode corresponds roughly to the ambipolar diffusion time. When a voltage is applied, the plasma center-of-mass shifts from the center of the diode. But whether that shift is towards the cathode or anode depends sensitively on the relative mobility of the plasma ions and electrons. Finally, we summarize the derivation of an analytic model of whistler wave excitation by an external dipole antenna. In addition, a dispersion relation is derived to estimate the plasma heating in the sheath due to plasma waves excited by the antenna.

Contents

I. INTRODUCTION

Hypersonic vehicles traveling in the upper atmosphere at speeds greater than Mach 10 (7,000 mph at 33 km altitude) generate plasma that disrupt or prevent communications over conventional radio-frequency channels. This phenomenon manifests itself most famously as the well-known communications "blackout" period during space vehicle reentry into the atmosphere [1–3], and has been studied (off and on) since the Gemini and Apollo space programs. For sustained hypersonic flight in the atmosphere, the communications blackout will persist for almost the entire flight.

The plasma boundary layer is formed around a hypersonic vehicle in the bow shock and to some extent by the collision of neutral gas particles with material ablated from the surface of the hypersonic vehicle itself. In the shock, the air is heated to such a high temperature that ionizing collisions between neutral particles occur. Estimates of electron density, n_p ($\sim 10^{12}$ cm^{-3}), temperature (~ 0.5 eV) and electron-neutral collision frequencies (2.5×10^9–42.5×10^{11} s^{-1}) have been obtained for high-Mach-number reentry vehicles at altitudes between 100,000-150,000 ft (30–45 km) [4, 5]. The thickness of the plasma layer (defined as the region where the electron density exceeds $\sim 10^9$ cm^{-3}) associated with these parameters is on the order of 6 cm, with 90% of the peak density out to a width of about 2 cm. The free electrons in the plasma layer attenuate radio-frequency (RF) waves both through reflection and resistive absorption, and generate RF noise. At sufficiently large antenna power levels, the RF itself can cause further ionization of the air to occur.

Acceptably low attenuation of electromagnetic (EM) wave propagation in a collisionless plasma is limited to frequencies above the cutoff value $f_c = \omega_{pe}/2\pi$, where ω_{pe} is the electron plasma frequency (see, for example, Ref. [6]). For $n_p = 10^{12}$ cm^{-3}, the $f_c \sim 10$ GHz, which

is at the high end of the radio wave frequency spectrum and well into the conventional microwave portion of the EM spectrum. In addition, this plasma cutoff frequency is above the spectrum allocated (in some cases by international treaty) for flight test and evaluation telemetry and above frequencies supported by existing infrastructure. We note that Global Positioning System signals are broadcast in the L-band region of the spectrum, and consequently are also heavily attenuated by the plasma sheath. As a result, communication approaches within the standard telemetry spectrum are inadequate for hypersonic vehicles using conventional techniques (see, for example, Refs. [6, 7]).

A theoretical research program is underway to assess concepts for real-time telemetric communications through plasma boundary layers surrounding hypersonic vehicles in flight. This research includes detailed analytic analysis and computational modeling of several proposed communication schemes. In our previous report [8], we summarized our research progress on three such schemes: a nonlinear three-wave interaction technique [9–11], an electron-acoustic wave (EAW) propagation scheme, and a magnetic window scheme for EM wave propagation through a collisional plasma slab. Here we summarize recent progress in our analysis of the EAW communication scheme (Sec. II). In a separate report [12], we present updated 2D numerical simulations of the magnetic window scheme and new 3D simulation results. These new simulations demonstrate the ability to model detailed, complex antenna structures which is an important aspect to all the communication schemes presently under analysis.

In Sec. III, we present the results of 1D particle-in-cell simulations of a plasma-filled cross-field diode. These simulations are intended to model some of the critical physical processes of the ReComm scheme for communications through the plasma sheath surrounding a hypersonic vehicle during re-entry. The ReComm scheme utilizes externally generated crossed

electric and magnetic fields to induce charged-particle drifts. This spatially redistributes the plasma and enables propagation of electromagnetic waves through the plasma layer. We demonstrate that the time required to significantly alter the plasma density profile in the diode corresponds roughly to the ambipolar diffusion time. When a voltage is applied, the plasma center-of-mass shifts from the center of the diode. But whether that shift is towards the cathode or anode depends sensitively on the relative mobility of the plasma ions and electrons.

In Sec. IV, we present analytic modeling of the whistler wave communication scheme. The impact of the antenna radiation field on the plasma sheath properties is assessed. A summary of our progress on the various communication schemes is given in Sec. V.

II. ELECTRON ACOUSTIC WAVE TRANSFORMATION

One scheme for communication through a plasma sheath is based on the possibility of propagating EAWs with frequencies well below the local plasma frequency ($\sim$ 9 GHz) in a two-electron-temperature plasma. A small hot electron population is produced by injection of an energetic electron beam. Over a certain range of wavelengths, the hot-electron component of the plasma can short out the electric fields that produce plasma oscillations in the cold plasma, thereby reducing the frequency of these oscillations below the cold plasma frequency. It may be possible to excite these electrostatic oscillations with an antenna and have them couple to electromagnetic RF oscillations outside the sheath. Related research was carried out in the CHARGE 2B ionospheric rocket experiments [13–15]. For sustained hypersonic flight, a comprehensive analysis is required to estimate the feasibility of this concept.

A. EAW to EM Wave Transformation at the Sheath Boundary

We use the hydrodynamic approximation to describe the transformation of an EAW into an EM wave at the plasma sheath boundary. This transformation is essentially the conversion of longitudinal EAWs propagating inside the plasma layer into EM waves propagating in the atmosphere.

We retain the two temperature plasma description, with the cold and hot electron temperatures denoted as T_c and T_h, respectively. The total electron plasma density is the sum of the hot and cold electron components, $N_e = n_c + n_h$. Density perturbations under the influence of the wave fields are denoted as $n_c = n_{0c} + \delta n_c$ and $n_h = n_{0h} + \delta n_h$, and electron velocity perturbations are denoted as δv_c and δv_h. We consider the transformation of an incident EAW with frequency

$$\omega_k = \omega_{pc}\left(1 + \frac{1}{k^2 r_{Dh}^2}\right)^{-1/2}, \tag{1}$$

propagating in the plasma layer into an EM wave propagating in air,

$$\omega_k = k\frac{c}{\sqrt{\epsilon_0}}. \tag{2}$$

[The notation used here follows Ref. [8]; e.g., ω_{pc} is the plasma frequency of the cold electrons and r_{Dh} is the Debye radius of the hot electrons.]

We assume that in the case of EAWs propagating in the plasma sheath, in the vicinity of the boundary there are two types of waves; EM waves with amplitude exponentially decreasing with increasing plasma density, and electrostatic EAWs propagating towards the boundary. In addition, we also take into account reflected EAWs and EM waves, propagating

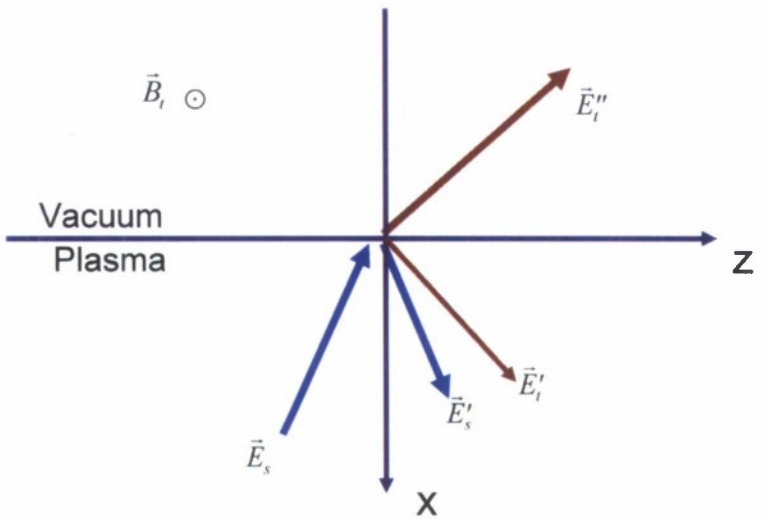

FIG. 1: Incident longitudinal and reflected EAWs (in blue with subscript s) and the transformed and reflected EM waves (in red with subscript t) of P-polarization (E_x, E_z, H_y).

in the air (see Fig. 1).

In order to derive equations for the transformation of EAWs at the boundary to P-polarized EM waves, we begin with Maxwell's equations:

$$\vec{\nabla} \times \vec{E} = -\frac{1}{c}\frac{\partial \vec{H}}{\partial t}, \tag{3}$$

$$\vec{\nabla} \times \vec{H} = \frac{1}{c}\frac{\partial \vec{E}}{\partial t} - \frac{4\pi e}{c}\left(n_{0c}\vec{v}_{1c} + n_{0h}\vec{v}_{1h}\right), \tag{4}$$

$$\mathrm{div}\vec{E} = -4\pi e\left(n_{1c} + n_{1h}\right). \tag{5}$$

The linearized equation of motion for the cold electrons can be written as

$$\frac{\partial \vec{v}_{1c}}{\partial t} = -\frac{e}{m}\vec{E} - \frac{1}{mn_{0c}}\vec{\nabla}P_{1c} - \nu_{ec}\vec{v}_{1c}, \tag{6}$$

where ν_{ec} is the cold electron-neutral collision frequency, and the (first-order) cold electron fluid pressure is expressed as

$$\vec{\nabla} P_{1c} = \gamma_0 m V_{Tc}^2 \vec{\nabla} n_{1c},$$

with γ_0 representing the adiabatic constant, and

$$V_{Tc}^2 = \sqrt{T_c/m}.$$

(Subscripts prefixed by "0" and "1" denote the usual zeroth and first order terms, respectively, in the linear expansion.) The linearized continuity equations for the cold electrons has the form

$$\frac{\partial n_{1c}}{\partial t} + n_{0c} \mathrm{div} \vec{v}_{1c} = 0. \tag{7}$$

Similarly for the hot electrons, the linearized equations of motion and continuity are

$$\frac{\partial \vec{v}_{1h}}{\partial t} = -\frac{e}{m}\vec{E} - \frac{1}{m n_{0c}} \vec{\nabla} P_{1h} - \nu_{eh} \vec{v}_{1h}, \tag{8}$$

$$\frac{\partial n_{1h}}{\partial t} + n_{0h} \vec{\nabla} \cdot \vec{v}_{1h} = 0, \tag{9}$$

with

$$\vec{\nabla} P_{1h} = \gamma_0 m V_{Th}^2 \vec{\nabla} n_{1h},$$

and

$$V_{Th}^2 = \sqrt{T_h/m}.$$

Equations (4) - (9) can be used to describe both (a) the transformation of an incident EM wave into an EAW inside the plasma sheath as well as (b) the transformation of an

EAW incident on the plasma/air boundary into an EM wave. Here we focus on these transformations at a relatively sharp boundary of a plasma sheath. If L is the characteristic distance over which the plasma density is decreasing from some finite value to zero and δ is the skin depth for EM field penetration into the plasma, then the condition for which the plasma boundary can be defined as sharp is simply $\delta \gg L$.

Applying the *curl* operator to Eq. (4) and using Eqs. (3) and (7), the following equation for the y-component of magnetic field in plasma can be obtained:

$$\frac{d^2 H_y}{dx^2} + \left(\frac{\omega^2}{c^2} \epsilon_c - k_{tz}^2 \right) H_y = 0, \tag{10}$$

where k_{tz} is the transformed EM wave vector (note that $k_{tz} = k_{sz}$), penetrating into the plasma sheath and

$$\epsilon_c = 1 - \frac{\omega_{pc}^2}{\omega^2}. \tag{11}$$

Taking into account that $\epsilon_c < 0$, we see from Eq. (11) that the magnetic field associated with the penetrated EM wave will exponentially decrease as the wave propagates in the x direction.

Now we can obtain expressions for the perturbed electron velocities $\vec{v}_{1c}$ and $\vec{v}_{1h}$ for use in Eq. (4). From Eqs. (6) and (7), it is straightforward to obtain the following expression:

$$\left[1 + \frac{\gamma_0 V_{Tc}^2}{\omega \left(\omega + i\nu_{ec} \right)} \vec{\nabla} \mathrm{div} \right] \vec{v}_{1c} = -i \frac{e}{m} \frac{1}{\omega \left(\omega + i\nu_{ec} \right)} \vec{E}. \tag{12}$$

Taking into account that for the cold plasma electrons:

$$\vec{E} \gg \frac{\gamma_0 V_{Tc}^2}{\omega \left(\omega + i\nu_{ec} \right)} \vec{\nabla} \mathrm{div} \vec{E}, \tag{13}$$

we can rewrite Eq. (12) for $\vec{v}_{1c}$ as

$$\vec{v}_{1c} = -i\frac{e}{m}\frac{1}{\omega\left(\omega + i\nu_{ec}\right)}\vec{E} + i\frac{e}{m}\frac{\gamma_0 V_{Tc}^2}{\omega\left(\omega + i\nu_{ec}\right)^2}\vec{\nabla}\mathrm{div}\vec{E}. \tag{14}$$

Introducing the linear operator, $\hat{L}_h$,

$$\hat{L}_h = 1 + \frac{\gamma_0 V_{Th}^2}{\omega\left(\omega + i\nu_{eh}\right)}\Delta, \tag{15}$$

and noting that for the hot electrons the second term in (15) is larger than the first one, from Eqs. (8) and (9) we can obtain the following expression for the linearized speed of the hot electrons in the plasma sheath:

$$\hat{L}_h\vec{v}_{1h} = -i\frac{e}{m}\frac{1}{\omega\left(\omega + i\nu_{eh}\right)}\left[1 + \frac{\gamma_0 V_{Th}^2}{\omega\left(\omega + i\nu_{eh}\right)}\Delta\right]\vec{E} + i\frac{e}{m}\frac{\gamma_0 V_{Th}^2}{\omega\left(\omega + i\nu_{eh}\right)^2}\vec{\nabla}\vec{\nabla}\cdot\vec{E}. \tag{16}$$

Now, applying the operator $\hat{L}_h$ to Eq. (4) and using Eqs. (14) and (16), we obtain the following equation:

$$\vec{\nabla}\times\left(\hat{L}_h\vec{H}\right) = -i\frac{\omega}{c}\left[\epsilon_c - \frac{\omega_{ph}^2}{\omega\left(\omega + i\nu_{eh}\right)}\right]\hat{L}_h\vec{E} - i\frac{\omega_{ph}^2}{c}\frac{\gamma_0 V_{Th}^2}{\omega\left(\omega + i\nu_{eh}\right)^2}\vec{\nabla}\mathrm{div}\vec{E}. \tag{17}$$

When applied to the transverse EM field, $\hat{L}_h \simeq 1$. Rewriting Eq. (3) as

$$i\frac{\omega}{c}H_y = ik_z E_x - \frac{dE_z}{dx}, \tag{18}$$

Eq. (17) can be expressed as:

$$\epsilon_c \frac{\gamma_0 V_{Th}^2}{c\left(\omega + i\nu_{eh}\right)} \frac{\partial^2 E_x}{\partial x^2} + \frac{\omega}{c}\left[\epsilon_c - \frac{\omega_{ph}^2}{\omega\left(\omega + i\nu_{eh}\right)}\right]\left(1 - \frac{\gamma_0 V_{Th}^2 k_{tz}^2}{\omega\left(\omega + i\nu_{eh}\right)}\right) E_x \tag{19}$$

$$= \left(1 - \frac{\gamma_0 V_{Th}^2 \omega_{ph}^2}{c^2\left(\omega + i\nu_{eh}\right)^2}\right) k_{tz} H_y,$$

$$\left[\frac{\omega_{ph}^2}{\omega\left(\omega + i\nu_{eh}\right)} - \epsilon_c\right] \frac{\gamma_0 V_{Th}^2}{\left(\omega + i\nu_{eh}\right)} \frac{\partial^2 E_x}{\partial x^2} + \left[\frac{\omega_{ph}^2}{\left(\omega + i\nu_{eh}\right)} - \epsilon_c\left(\omega - \frac{\gamma_0 V_{Th}^2 k_{tz}^2}{\left(\omega + i\nu_{eh}\right)}\right)\right] E_z \tag{20}$$

$$-ik_{tz} \frac{\gamma_0 V_{Th}^2 \omega_{ph}^2}{\omega\left(\omega + i\nu_{eh}\right)^2} \frac{\partial E_x}{\partial x} = -ic \frac{\partial H_y}{\partial x}.$$

The system of equations (10), (19) and (20) describes the transformation of an EAW incident onto the plasma/air interface from within the plasma into an EM wave. In addition, this same system of equations describes the transformation of EM wave incident from the air into EAW propagating inside the plasma sheath.

B. Solution Set

Transformation of EAW waves on the sheath boundary can be described by the equations (10), (19), and (20). Solution of these equations can be presented in the form:

$$H_{1y} = -\frac{\omega}{ck_{1zt}} \epsilon_{tot} G E_1 \exp\left(-\kappa'_{1tx} x\right), \tag{21}$$

$$E_{1x} = E_1 \exp\left(-iq_1 x\right) - G E_1 \exp\left(-\kappa'_{1tx} x\right), \tag{22}$$

$$E_{1z} = -E_1 \frac{k_{1sz}}{q_1} \exp(-iq_1 x) + iG \frac{\kappa'_{1tx}}{k_{1tz}} E_1 \exp\left(-\kappa'_{1tx} x\right), \tag{23}$$

$$H_{2y} = -\frac{\omega}{ck_{1zt}} \epsilon_{tot} G E_2 \exp(-\kappa'_{1tx} x), \tag{24}$$

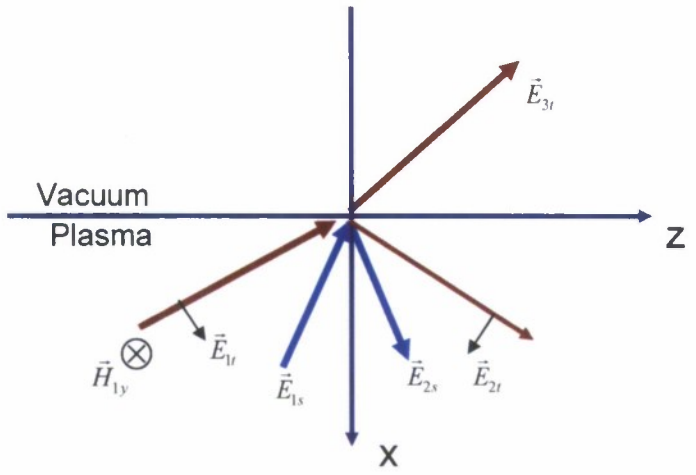

FIG. 2: Incident longitudinal and reflected EAW waves (in blue with index s) and transformed and reflected electromagnetic waves (in red with index t) of P-polarization (E_x, E_z, H_y).

$$E_{2x} = E_2 \exp(iq_1 x) - GE_2 \exp(-\kappa'_{1tx} x), \tag{25}$$

$$E_{1z} = E_2 \frac{k_{1sz}}{q_1} \exp(iq_1 x) + iG \frac{\kappa'_{1tx}}{k_{1tz}} E_2 \exp(-\kappa'_{1tx} x). \tag{26}$$

In the solution set (21) - (26), the following notations are used (see Fig. 2):

$$\epsilon_{tot} = 1 - \frac{\omega_{pc}^2}{\omega(\omega + i\nu_{ec})} - \frac{\omega_{ph}^2}{\omega(\omega + i\nu_{eh})}; \tag{27}$$

the constant G is defined as:

$$E_{1,2tx} = GE_{1,2sx}, \tag{28}$$

where for $E_{1,2}$ we have

$$E_{1,2} = |E_{1,2sx}|, \tag{29}$$

$$\kappa'_{1tx} = \frac{\omega}{c} \sqrt{|\epsilon_c| + \sin^2 \theta_3}, \tag{30}$$

where θ_3 is the angle of the transmitted EM wave with respect to the plasma-vacuum interface normal, and we make use of the conditions

$$k_{1sz} = k_{1tx} = k_{2sz} = k_{2tz} = k_{3tz} = \frac{\omega}{c} \sin\theta_3. \tag{31}$$

Finally for q_1 we have

$$q_1 = |k_{1sx}|. \tag{32}$$

To find G we use the boundary condition for the speed of cold and hot electrons; that the normal component of hydrodynamic speed of hot and cold electrons is zero on the boundary:

$$v_{hx}(0) = 0, \quad v_{cx}(0) = 0. \tag{33}$$

This means that the electrons are elastically reflected from the boundary. Using the equations of motion for the cold and hot electrons and the Poisson equation, we write the following condition for the normal component of the electric field on the plasma sheath boundary:

$$\frac{\delta}{\delta x}\mathrm{div}\vec{E} = \frac{1}{R_D^2}E_x, \quad \text{at } x = 0, \tag{34}$$

where for R_D is

$$\frac{1}{R_D^2} = \frac{1}{r_{Dc}^2} + \frac{1}{r_{Dh}^2}.$$

Boundary condition (31) allows us to determine the constant G, which connects E_{1xt} with E_{1sx},

$$G = 1 + \frac{R_D^2}{r_{Dh}^2}\frac{1}{|\epsilon_c|}. \tag{35}$$

The boundary conditions for the magnetic field are

$$H_{1y}(0) = H_{2y}(0) = H_{3y}(0), \tag{36}$$

and the electric field are

$$E_{1z}(0) + E_{2z}(0) = E_{3z}(0). \tag{37}$$

Using Eqs. (21) - (26), we obtain the following expressions for the magnitudes of reflected EAW (E_2) and transmitted EM waves (E_3):

$$E_2 = \frac{Z_1 - \cos\theta_3}{\cos\theta_3 - Z_2}, \tag{38}$$

$$E_3 = \frac{Z_1 - Z_2}{\sin\theta_3(Z_2 - \cos\theta_3)}\epsilon_{tot}E_1. \tag{39}$$

From the boundary conditions, the impedances Z_1 and Z_2 can be obtained:

$$Z_1 = \frac{E_{1z}(0)}{H_{1y}(0)} = -i\frac{c\kappa'_{1tx}}{\omega\epsilon_{tot}} + \frac{\omega\sin^2\theta_3}{cq_1G\epsilon_{tot}} \tag{40}$$

$$Z_2 = \frac{E_{2z}(0)}{H_{2y}(0)} = -i\frac{c\kappa'_{2tx}}{\omega\epsilon_{tot}} + \frac{\omega\sin^2\theta_3}{cq_2G\epsilon_{tot}}. \tag{41}$$

Now the coefficient of transformation in amplitude of an electron acoustic wave inside a plasma sheath into an electromagnetic wave propagating in the air can be written as:

$$\frac{E_3}{E_1} = \left(\frac{2\omega}{cq_1}\right)\frac{|\epsilon_{tot}|\sin\theta_3}{[\omega/(cq_1G)]\sin^2\theta_3 - |\epsilon_{tot}|\cos\theta_3 + i\sqrt{|\epsilon_c| + \sin^2\theta_3}}. \tag{42}$$

In the process of derivation of (42), we also assumed that $\nu_{ec} \ll \omega$.

The power associated with the transformation of an EAW into an EM wave can be defined as the ratio of the normal component of the energy density flux of an EM wave:

$$S_{EM} = c\frac{E_3^2}{4\pi}\cos\theta_3 \tag{43}$$

to the normal component of the energy density flux of an EAW:

$$S_{\perp EAW} = S_{EAW}\cos\theta_1 \sim S_{EAW}, \tag{44}$$

and for S_{EAW} we have

$$S_{EAW} = V_g\frac{\delta}{\delta\omega}(\omega\epsilon_s)\frac{E_s^2}{8\pi}, \tag{45}$$

where V_g is the wave group velocity. Here E_s is the electrostatic field magnitude for the EAW and

$$\epsilon_s = 1 + \frac{1}{k_s^2 r_{Dh}^2} - \frac{\omega_{pc}^2}{\omega^2}.$$

From (45) we obtain

$$S_{EAW} = \frac{1}{k_s r_{Dh}}\frac{\omega_{pc}}{k_s}\frac{E_s^2}{4\pi}. \tag{46}$$

Using Eqs. (44) and (46), the transformation coefficient W_T:

$$W_T = 16\pi\frac{V_{Th}}{c}\frac{\omega_{pc}}{\omega_{ph}}\frac{|\epsilon_{tot}|^2}{|\epsilon_c|^2}\frac{1}{q_1^2 r_{Dh}^2}\frac{\cos\theta_3\sin^2\theta_3}{\left[\omega/\left(cq_1G\right)\sin^2\theta_3 - |\epsilon_{tot}|\cos\theta_3\right]^2 + \left(|\epsilon_c| + \sin^2\theta_3\right)}. \tag{47}$$

To obtain (47), we also used:

$$|\epsilon_c| = \frac{1}{k_s^2 r_{Dh}^2} = 1 - \frac{\omega_{pc}^2}{\omega^2}. \tag{48}$$

Taking into account that $\cos\theta_{1s} \sim 1$ and $|\epsilon_{tot}| \sim |\epsilon_c|$, we can replace (47) by:

$$W_T = 16\pi\,|\epsilon_c|\,\frac{V_{Th}}{c}\frac{\omega_{pc}}{\omega_{ph}}\frac{\cos\theta_3\sin^2\theta_3}{\left[\omega/\left(cq_1G\right)\sin^2\theta_3 - |\epsilon_{tot}|\cos\theta_3\right]^2 + \left(|\epsilon_c| + \sin^2\theta_3\right)}. \tag{49}$$

In the next section we investigate the dependence of the transformation coefficient W_T from the propagation angle θ_3 of an outgoing electromagnetic wave propagating outside the plasma sheath.

C. Numerical Evaluation of the Transmitted Power

In the previous section, the angular dependence of the transformation coefficient W_T of an EAW propagating inside a plasma sheath into an EM wave propagating outside the plasma sheath was obtained [Eq. (47)]. Taking into account that $\cos\theta_{1s} \sim 1$ and $|\epsilon_{tot}| \sim |\epsilon_c|$, Eq. (49) was obtained. In our analysis of this expression, we use the following notations:

$$a_1 = \frac{V_{Th}}{c}, \quad a_2 = \frac{\omega_{pc}}{\omega_{ph}}, \quad a_3 = \frac{\omega}{cq_1} = \frac{V_{Th}}{c}\frac{\omega_{pc}}{\omega_{ph}} = a_1a_2,$$

$$q_1 = |k_{1sx}| = k_{1s}\cos\theta_{1s} \sim k_{1s} = \frac{1}{r_{Dh}}\frac{1}{\sqrt{\left(\omega_{pc}^2/\omega^2\right) - 1}}.$$

Considering $\nu_{ec} \ll \omega$ and $\nu_{eh} \ll \omega$ for $|\epsilon_{tot}|$, we can simply write:

$$|\epsilon_{tot}| = \frac{\omega_{pc}^2 + \omega_{ph}^2}{\omega^2} - 1.$$

Now we can rewrite the expression for the transformation coefficient [Eq. (49)]in the form:

$$W_T = 16\pi|\epsilon_c|\;a_1a_2\frac{\cos\theta_3\sin^2\theta_3}{\left(a_3G^{-1}\sin^2\theta_3 - |\epsilon_{tot}|\cos\theta_3\right)^2 + \left(|\epsilon_c| + \sin^2\theta_3\right)}. \tag{50}$$

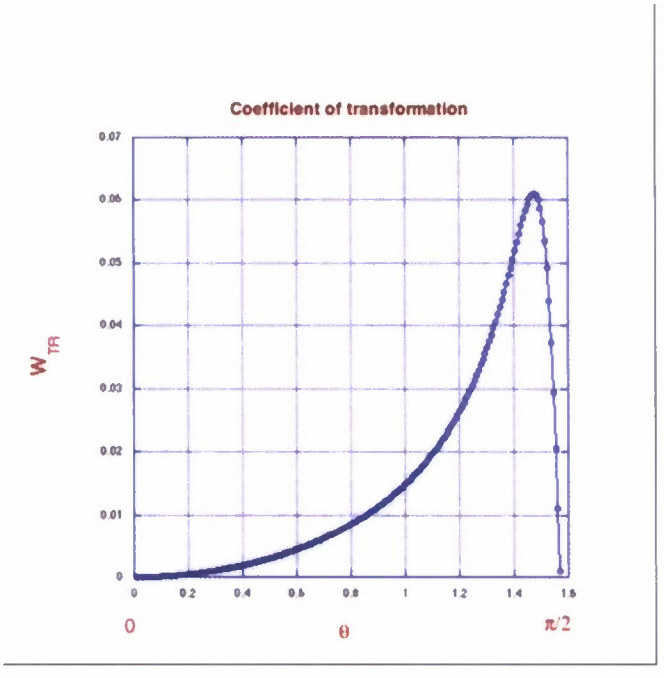

FIG. 3: Dependence of the transformation coefficient from the propagation angle (angle between the direction of the EM wave propagation and the normal to a plasma sheath) of an outgoing EM wave.

Equation (50) is numerically evaluated (see Appendix A) to plot the dependence of W_T on the EM wave transmission angle θ_3. We find in Fig. 3 that the transformation coefficient is large for large propagation angles of the outgoing EM wave. The transmitted power is a maximum for propagation angles close to $\pi/2$ (EM waves propagating almost parallel to the plasma sheath boundary). This is different from the case of Langmuir wave transformation into an EM wave at the plasma boundary, where the transformation coefficient is large for small propagation angles of the outgoing EM wave. We note that the magnitudes of these transformation coefficients are comparable in both the Langmuir wave and EAW cases.

III. 1D ANALYSIS OF THE RECOMM SCHEME

We present the results of 1D particle-in-cell (PIC) simulations of a plasma-filled cross-field diode using the LSP code[16]. These simulations are intended to model the ReComm

scheme[17] for communications through the plasma sheath surrounding a hypersonic vehicle during re-entry. As is well known, an electromagnetic wave at angular frequency ω can only propagate through a thick collisionless plasma with a density low enough so that the plasma frequency $\omega_p \propto \sqrt{n}$ does not exceed ω. In certain altitude ranges the density in the shock induced plasma layer surrounding hypersonic vehicles is high enough to attenuate RF signals in the L band ($f \sim 1 - 3$ GHz) which is used for telemetry and evaluation (T&E).

A simplified picture of the ReComm scheme can be seen in Fig. 4. The antenna aperture is placed in between a pair of biased electrodes. An electromagnet provides a magnetic field normal to the antenna aperture throughout the region between the electrodes. We consider in this report the "plasma-optic" regime described by Keidar *et al.* [18] in which electrons are magnetized and ions are unmagnetized. The separation distance between the plates, L, is assumed to be large compared to the electron Larmor radius, but small with respect to the ion Larmor radius. In this case, if $\mathbf{E}$ is the electrostatic field between the electrodes, the electrons are line-tied and can only $\mathbf{E} \times \mathbf{B}$ drift parallel to the electrodes. In principle [18, 19], this prevents the electrons from screening out the electric field in the bulk of the plasma between the electrodes. The ions, being unmagnetized, are then accelerated in the unscreened electric field. This simple description assumes that electrons are collisionless. If there is a finite electron-ion and/or electron-neutral collision frequency, the electrons can diffuse across field lines. Including both ion and electron collisionality in a 1D fluid theory analysis, Keidar *et al.* argue that a steady-state spatial distribution results in which the plasma density is reduced near the anode side. The amount of density reduction will be a function of the plasma properties, electrode voltage, and magnetic field strength. The aperture of the antenna used for communications would then be placed directly below the reduced density region, where the plasma frequency will be lower. A communication

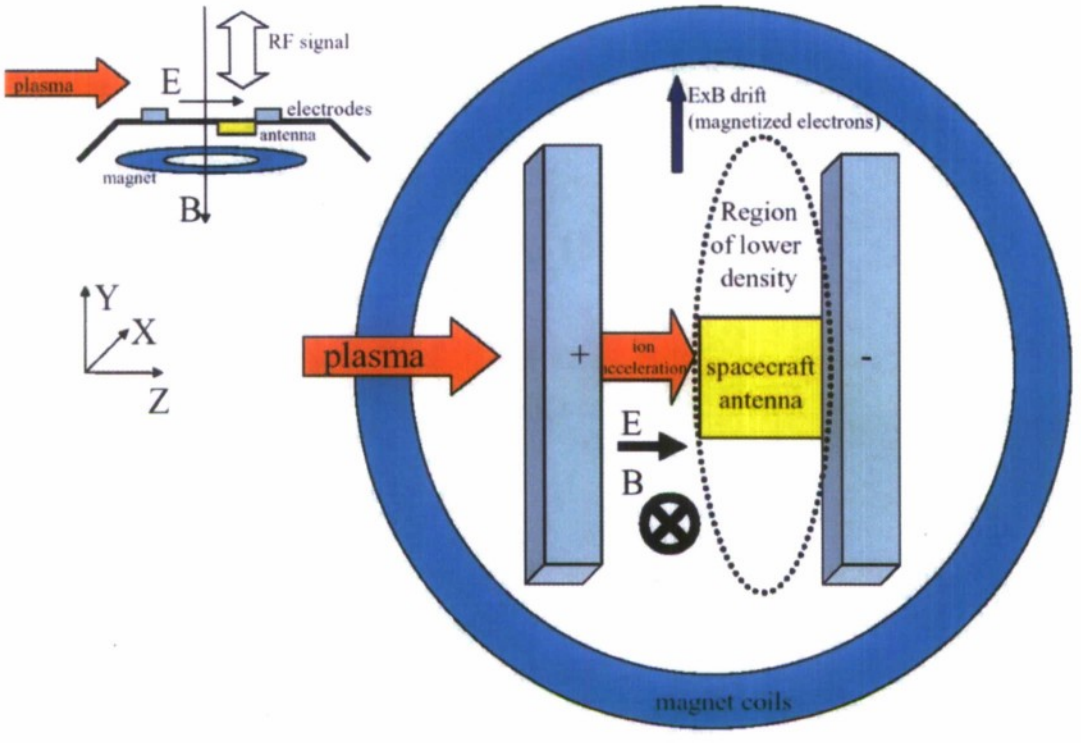

FIG. 4: ReComm communication through plasma layer using applied electric and magnetic fields. Adapted from Ref. [17].

frequency of 1 GHz corresponds to a free-space wavelength of 30 cm. The antenna aperture will be on the order of the wavelength, which means, as a rough estimate, we can assume that the electrode separation L must be on the order of a meter.

In this report we describe the results of 1D simulations of cross-field parallel-plate simulations in the plasma-optic regime. We consider only the issue of the temporal evolution of the plasma density in the region between the electrodes due to the applied voltage and magnetic field. The details of electromagnetic wave propagation through the finite-thickness plasma sheath are not considered. 2D and 3D effects are neglected for the present. In Sec. III A we describe results from a baseline ReComm simulation using parameters believed to be consistent with those in the radio blackout regime. The simulation results suggest that the

Plate separation	L (cm)	1.0
Applied voltage	V (V)	100
Applied magnetic field	B (G)	2000
Initial plasma density	n (cm^{-3})	10^{11}
Initial Electron temperature	T_e (eV)	10.0
Initial Ion temperature	T_i (eV)	0.1
Ion-neutral collision frequency	ν_{in} (ns^{-1})	0.066
Electron-neutral collision frequency	ν_{en} (ns^{-1})	0.329

TABLE I: Physical parameters for the baseline 1D ReComm simulation. A spatially uniform singly ionized Ar plasma is placed between plate electrodes. Results from the simulation are shown in Fig. 5.

system behaves roughly like an ambipolar diffusion process, and that the temporal evolution of the plasma occurs on corresponding time scales. In Sec. III B we describe the results of a series of parametric studies in which diode length, voltage, and plasma collisionality are varied from the baseline simulation values.

A. 1D Simulations

The simulations consist of a 1D grid with conductors at the boundaries. A constant voltage difference (after a short temporal ramp) of V is applied between the cathode ($x = 0$) and anode ($x = L$). Table I shows the physical parameters used in what we will refer to as the "baseline" ReComm simulation. In this section we will discuss results from this single baseline simulation. Results from a series of parametric studies, in which various parameters are varied from the baseline values, will be discussed in the following section.

An initially-uniform singly-ionized Ar plasma is placed between the plates. The plasma density of 10^{11} cm^{-3} corresponds to an electron plasma frequency of $\omega_{pe} \simeq 20$ GHz which is much larger than the L-band frequencies available for T&E purposes. We assume that

the plasma is initially at rest with respect to the electrodes. That is, we assume that plasma physics phenomena of interest occur on time scales short compared to the ratio of the plate separation and the hypersonic flow velocity. We will consider the validity of this assumption later in the report. Ion-neutral and electron-neutral collisions are included in the PIC simulations by a Monte-Carlo collision model which has been described in detail elsewhere[20–22]. For simplicity we have assumed a constant ion-neutral (ν_{in}) and electron-neutral (ν_{en}) collision frequency (the collision frequency should, of course, in general be a function of the particle energy). Ionization and other more complicated gas chemistry effects are neglected for the present. For this reason, it is not very significant that we have replaced the N_2 and O_2 molecular ions species which comprise the bulk of an air plasma with Ar ions, which are only slightly heavier. The electron-collision frequency value used in the baseline simulation corresponds to a value of $\nu_{en} \simeq 0.02\omega_{pe}$, which is in accord with estimates of the value in the hypersonic plasma sheath [6, 12]. Since we have not found any experimental data or estimates for the ion-neutral collision frequency, we have chosen to set $\nu_{in} = \omega_{pi}$, where ω_{pi} is the ion plasma frequency. We note that a collision frequency of this order was found to damp ion-acoustic waves driven by sheath oscillations near the cathode and anode surfaces in initial simulations with negligible electron collisionality.

For these initial 1D simulations we wanted to attempt to resolve electron time and length scales while also allowing the simulations to run out long enough to observe ion dynamics. For this reason we began with a relatively small plate separation value of $L = 1$ cm. If we estimate the electric field in the gap by V/L and apply a 2000 G magnetic field as shown in Table I, the $\mathbf{E} \times \mathbf{B}$ drift velocity is $v_D \sim 5 \times 10^4$ m/s, which is about 10 times larger than the ion thermal velocity v_{ti} and 10 times smaller than the electron thermal velocity v_{te}

$(v_{ti} < v_D < v_{te})$. For each plasma species s $(= e$ or $i)$ we define the Larmor radius as

$$r_{Ls} = \frac{\max\left[v_D, v_{ts}\right]}{\omega_{cs}}, \tag{51}$$

where ω_{cs} is the cyclotron frequency of species s. We find that for the parameters in the table $r_{Le} \simeq 0.04$ cm and $r_{Li} \simeq 10$ cm, so these parameters are seen to be in the plasma-optic regime for a plate separation of 1 cm. We note that for this field value the electrons will still make many cyclotron orbits in between collisions, as $\nu_{en}/\omega_{ce} \sim 0.01$. By contrast the ions are in the opposite regime: $\nu_{in}/\omega_{ci} \sim 100$.

By choosing a plate separation of 1 cm, we can choose a cell size of $\Delta x = 0.04$ cm, which is on the order of the electron cyclotron radius, without requiring a prohibitively large number of computational grid cells. Several hundred plasma particles per cell were used in these simulations to provide a good statistical representation of the electron and ion energy distribution functions. Macro particles which strike the conducting boundaries are removed from the simulation without replacement. A time step of $\Delta t = 0.025$ ns gives $\omega_{ce}\Delta t \sim 2\omega_{pe}\Delta t \sim 0.9$, ensuring numerical stability. Simulations with this time step value agree well with simulations at smaller time step values, however, a significantly larger time step would require the use of implicit algorithms (Ref. [23] describes a new algorithm which allows numerically stable simultaneous under-resolution of ω_p and ω_c). This would probably be required for larger scale simulations (*i.e.*, 2D) than those presented here. The shortest ion timescale is given by $\omega_{pi}^{-1} \sim 15$ ns, so the simulations must be run for many time steps to follow the ion dynamics.

Figure 5 shows plots of ion density (top) and potential (bottom) across the anode-cathode gap from the baseline simulation at several time values. At $t = 50$ ns (a few ion plasma

periods), the ion density is uniform except at the electrode surfaces where the usual Debye sheaths have been established. The potential profile at 50 ns shows that electric field across the bulk of the plasma is fairly constant and $\sim V/L$. Locally, near the anode and cathode the potential decreases as the surface is approached, so the electrons are held back by local sheath electric fields. In general the sheath electric fields adjust themselves to repel the more mobile species. In this way quasi-neutrality can be maintained in the plasma. The potential drops near the conducting surfaces are of the order of the electron temperature.

As time increases, the ion density profile slowly evolves to a roughly sinusoidal shape, although the position of maximum ion density shifts towards the cathode in this case. So there is a shifting of the center-of-mass of the plasma towards the cathode side. However, significant changes in the ion distribution occur only on time scales of $\sim 10\ \mu$s. This requires the simulation to be runs for $\sim 10^6$ time steps. At these much later times there is no longer a (roughly) constant electric field in the bulk plasma. There is a fairly small electric field on the cathode side of the simulation with a larger electric field ($> V/L$) near the anode. We note that, other than the slight skewing of the density distribution toward the cathode, the general temporal behavior resembles that of a simple 1D ambipolar diffusion problem between parallel plates without an applied voltage.

This situation is discussed at some length in Ref. [24]. In Appendix B we extend the analysis of Ref. [24] to include the effects of an applied voltage. In the theory outlined in Appendix B the total plasma number density is assumed to decrease exponentially with a time constant of τ for the lowest order diffusion mode. We show in the following section, that this is approximately the case for the simulations presented in this report. For given geometry and plasma properties, the time constant τ can be calculated as a function of the three voltage scales, the applied voltage V, the ambipolar potential V_a [Eqs. (B5) and

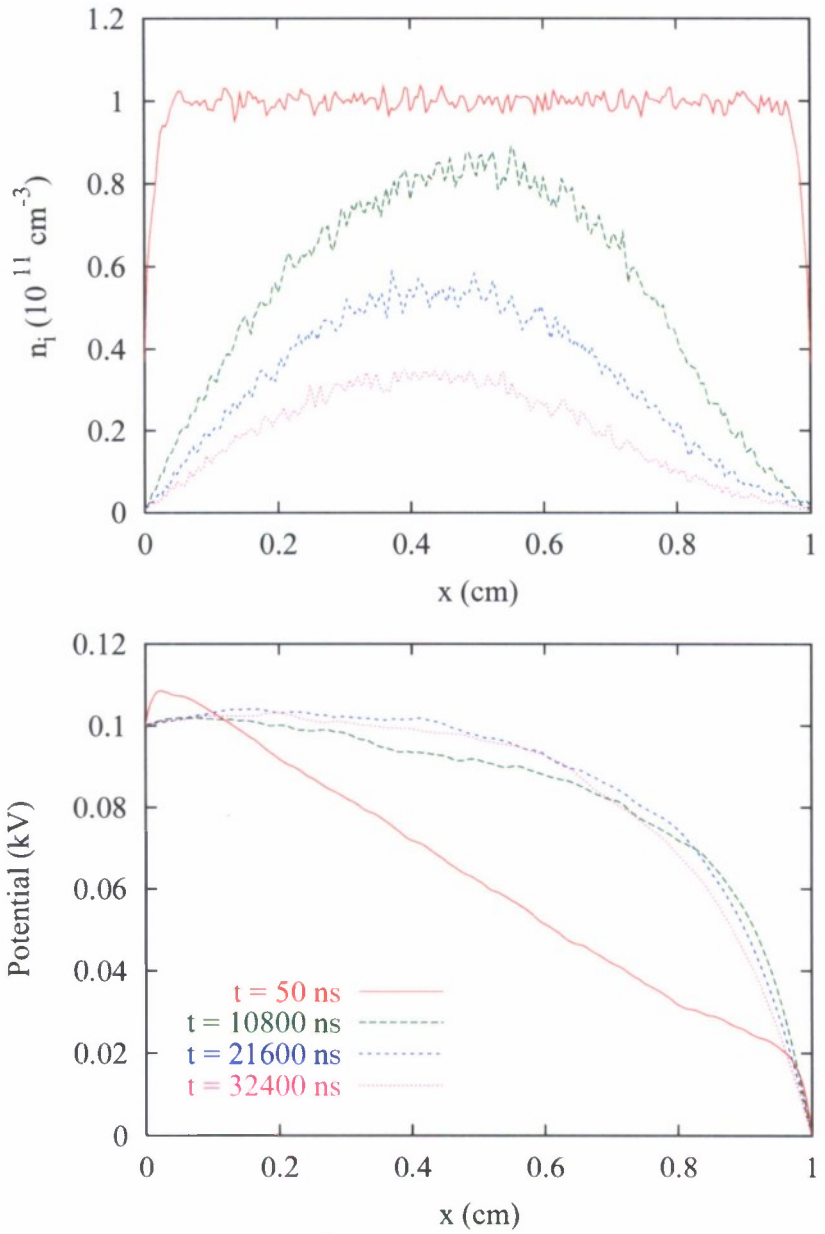

FIG. 5: Snapshots of ion density (top) and potential (bottom) as a function of x at several times for the baseline 1D ReComm simulation with parameters given in Table I.

(B7)], and V_M, the potential difference between the center of the diode and the cathode [Eq. (B13)]. The applied voltage V is, of course, a known input parameter. The ambipolar potential V_a is uniquely determined by the bulk plasma properties and is assumed to be

constant in the simple diffusion theory, and so can in principal be calculated from the initial conditions of the plasma. But the mid-potential V_M cannot be determined from a quasi-neutral diffusion theory and depends on the details of sheath physics at electrode surfaces. In the usual treatment of ambipolar diffusion it is approximated that $|V_M/V_a| \gg 1$ (this is equivalent to the statement that the plasma density at the electrodes is vanishingly small at the electrodes), the timescale τ is given approximately by

$$\tau = \left(\frac{L}{\pi}\right)^2 \frac{1}{D_a}, \tag{52}$$

where D_a is the ambipolar diffusion coefficient defined by Eqs. (B6) and (B7) [see Appendix A]. If we calculate τ using the parameters in Table I, we obtain $\tau \sim 50\mu$s. This simple estimate yields a timescale ~ 10 μs, which is in rough accord with the simulation results. Again using the parameters of the table, we can also estimate $V_a \sim -5.6$ eV. The analysis in Appendix B demonstrates that when an applied voltage is present and $V_a < 0$ (meaning that the electrons are more mobile), the center of mass of the density distribution should shift towards the cathode. This is also observed in the baseline simulation (Fig. 5).

We note that the diffusion theory outlined in Appendix B makes the assumption that both V_a and D_a are independent of both position and time. This implies that electron and ion temperatures and collision frequencies are constant as well. We consider now the time variation of the temperature. Figure 6 shows the electron and ion temperature (in units of volts) as well as V_M and V_a (calculated by using instantaneous values of temperature) as a function of time. We note that the temperature histories shown here represent a measure of velocity spread over the entire simulation space. Any spatial variations in temperature are averaged out in this process.

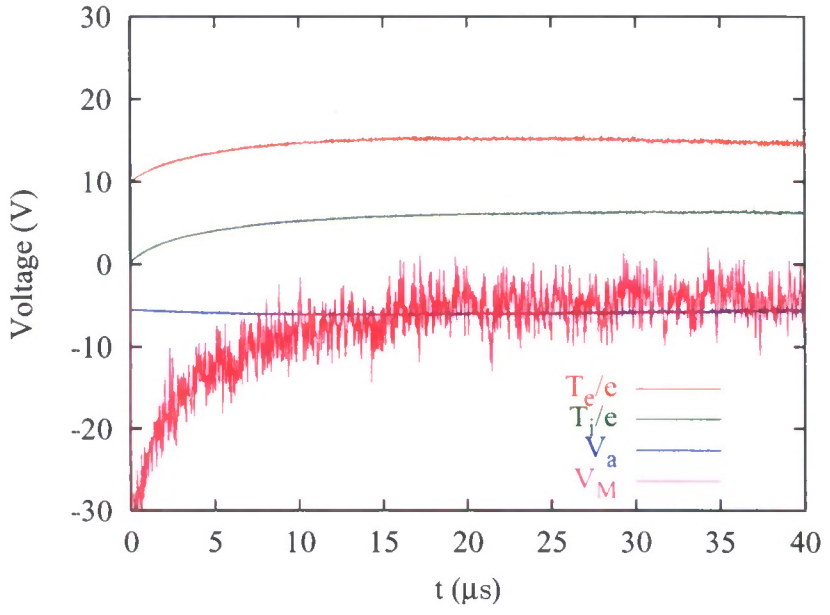

FIG. 6: Spatially averaged electron and ion temperatures and voltage scales as a function of t for the baseline 1D ReComm simulation with parameters given in Table I. The ambipolar voltage scale V_a is defined by Eq. (B5), and V_M is the potential difference between the center and the cathode [Eq. (B13)].

From Eq. (B8) we see that V_a is a linear combination of T_e and T_i (for fixed magnetic field and collision frequencies). Note that V_a can be positive or negative depending on the relative mobility of ions and electrons. The simple diffusion theory outlined in the appendix, assumes that both V_a and the diffusion coefficient D_a are constant in space and time. This implies that plasma temperatures and collision frequencies are constant. While collision frequencies are fixed by the code, we see from Fig. 6 that the average simulation temperatures exhibit some heating until about 10 μs, after which they level off. We restrict our consideration to times greater than 10 μs and neglect the time dependence.

When using the initial temperatures, we find that $V_a \sim -5.6$ eV. If we use instead the asymptotic temperatures, $T_e \sim 15$ eV and $T_i \sim 6$ eV, the ambipolar potential changes only slightly $V_a \sim -6$ eV. From the simulation we have an asymptotic value of $V_M \sim V_a$. As

shown in Appendix B, for $|V/V_a| \gg 1$, a physical solution to the diffusion equation requires that $V_M/V_a < ln(2)$. From Fig. 6, this clearly not the case.

This apparent contradiction can be explained as follows. We again emphasize that in Fig. 6 V_a is calculated by using spatially averaged values of the species temperatures. Since the electric fields are not uniform across the gap, there is actually an x variation in temperature due to non-uniform Joule heating. This can be seen in Fig. 7, where the bottom plot shows the electron and ion temperatures (in units of volts) as a function of x at $t = 20$ μs. We see that electrons are heated fairly uniformly across the gap, but ions are heated preferentially on the anode side, where the electric field is largest. We have also plotted V_a, calculated by Eq. (B6) using the local values of temperature, as a function of x. The spatial variation in V_a (and D_a) implies that the system no longer satisfies a simple diffusion equation.

The upper plot of Fig. 7 shows both the electron and ion density distributions at $t = 10$ μs. The data, which come from an instantaneous snapshot, are somewhat noisy. But it is clear that there is a significant charge imbalance occurring in a region which extends from the anode about 2 mm into the bulk plasma. This is therefore a large region (much larger than a Debye length) where the assumption of charge neutrality does not hold. In this same region V_a is positive, which implies that, at least locally, the ions are more mobile than the electrons. From ambipolar theory this would predict an ambipolar field in this region which would hold back the electrons from the anode, which is clearly not the case (as seen from the potential plot). But the large electric field is not ambipolar, since there is a significant charge imbalance. Alternately, in this region electron and ion fluxes are not nearly equal. This flux imbalance is required to draw current from the cathode to the anode.

As discussed in Appendix B, the simple diffusion theory also predicts a constant ion

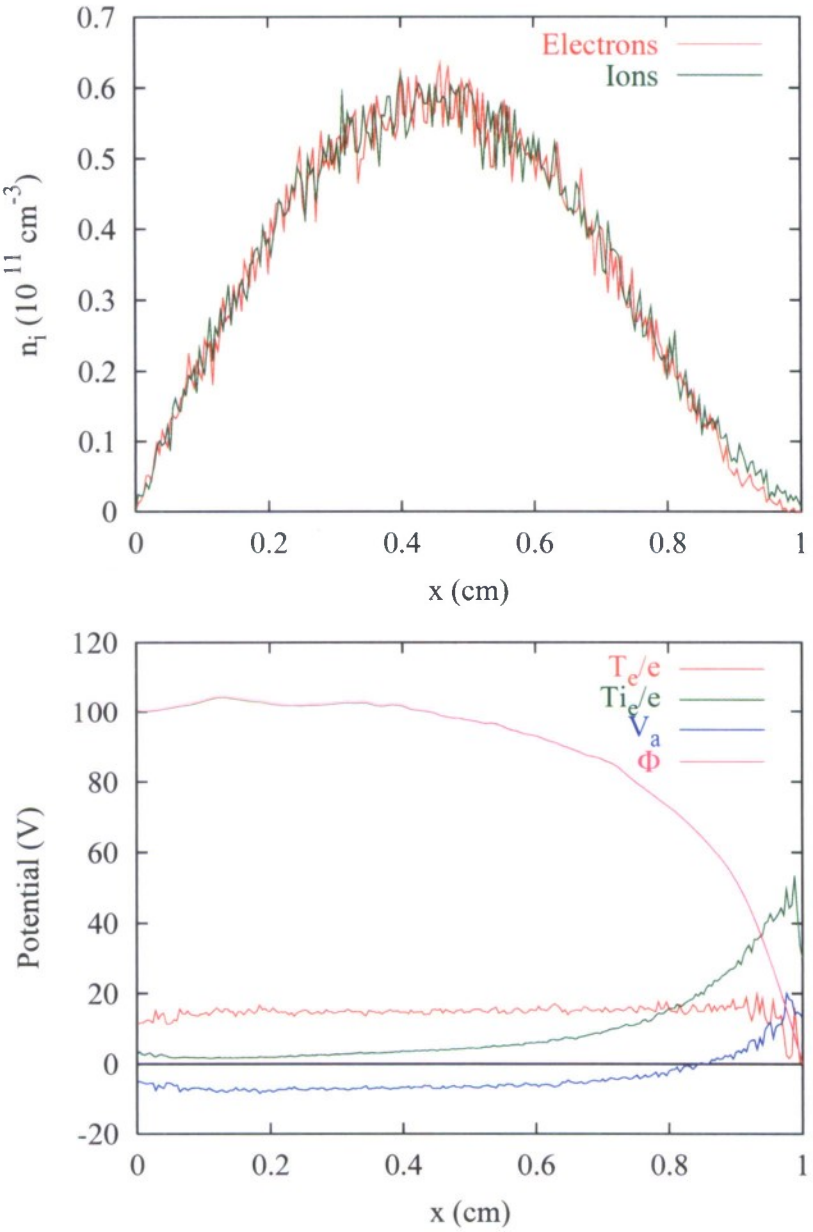

FIG. 7: Results from the baseline simulation at $t = 20$ μs. (Top) Ion and Electron density profiles. (Bottom) Ion and Electron temperature, V_a, and the electrostatic potential Φ (all in units of volts) as a function of x.

center-of-mass once the higher-order modes have decayed, although the density profiles in Fig. 5 exhibit a continuing drift of the center-of-mass at late times. This can also be explained by the fact that V_a and D_a are not spatially uniform. In this case it is no longer possible

to exactly separate the variables x and t of the density function, as in done Eq. (B9). The combination of this effect and the breakdown of quasi-neutrality leads to a time dependence in the position of the plasma center-of-mass. This is seen more clearly in the simulation results presented in Sec. III B.

We have demonstrated here that qualitatively our baseline ReComm simulation behaves as an ambipolar diffusion process, in which the density profile evolves on time scales consistent with diffusion theory. The density profile evolves to a roughly sinusoidal shape, in which the center-of-mass is shifted due to the applied voltage. The existence and sign of this shift can also be predicted by the simple diffusion theory. As we have demonstrated, however, there is significant Ohmic heating and large-scale charge separation present in the simulations, which preclude using the theory quantitatively. In the following sections we present the results of a series of parametric studies in which the input parameters of the ReComm simulation are varied systematically.

B. Parametric Studies

In this section we describe the results of parametric studies in which certain physical parameters are varied from the baseline values of Table I. We begin by describing the results from a series of simulations in which the electrode separation L is varied. All other physical parameters remain unaltered from the values in the table. We pointed out in the previous section that on long time scales the time evolution of the plasma density distribution resembles an ambipolar diffusion process. The timescale for a standard ambipolar diffusion process (*i.e.*, with no applied field) should scale as L^2/D_a. Figure 8 shows results for simulations with $L = 0.5, 1, 1.5, 2, 3$, and 4 cm. As mentioned above, the ion Larmor radius for the present set of input plasma parameters and magnetic field is ~ 10 cm. Simulations

with larger plate separations would require a decrease of the magnetic field strength to remain in the plasma-optic regime. Since the cell size Δx has been maintained for all these simulations, runs at larger values of L are also more time consuming. The top plot shows the total simulation ion charge $Q(t)$ [normalized by the initial charge value $Q(0)$] as a function of time. For all values of L, after a transient time, the total ion charge decreases exponentially. This is consistent with diffusion of the lowest order mode.

In the diffusion model, when higher order diffusion modes have decayed away, $Q(t)$ is proportional to the integral over x of $n(x,t)$, as given by Eq. (B9) of Appendix B. So after the transient time, the total ion charge can be expressed as

$$Q(t) \propto e^{-t/\tau_f}. \tag{53}$$

For each simulation, the timescale τ_f is found numerically by fitting the results for $Q(t)$. An alternate timescale can also be calculated from the first e-folding time of the total ion charge:

$$Q(\tau_e)/Q(0) = e^{-1}, \tag{54}$$

where $Q(0)$ is the initial ion charge. Both τ_f and τ_e are plotted as a function of L (the anode-cathode gap spacing) in the bottom plot. For the smaller values of L both τ values scale approximately as L^2, but for $L > 2$ cm, the quadratic scaling falls off to something closer to a linear dependence. This can be explained by referring to ambipolar diffusion theory. As shown in Appendix B, the dimensionless parameter $L^2/D_a\tau$ is a function of both V/V_a and V_M/V_a. D_a and V_a are functions only of the bulk plasma parameters, however, the mid potential V_M, which cannot be determined by simple quasi-neutral fluid theory, is in general a function of L. This L dependence, which can be seen in the bottom plot of

Fig. 9, breaks the simple scaling relation $\tau \propto L^2$.

Figure 9 shows the ion density and potential for each simulation as a function of x/L at the time $t = \tau_e$. The density profiles have a nearly self-similar shape, except for a slight shifting of the ion center-of-mass back toward the center of the diode with increasing L. The potential profiles have qualitatively the same shape, but the mid potential V_M increases somewhat with increasing L. We also note that for each run the mid potential V_M is roughly constant in time after a transient time of order τ_e. The same is also roughly true of the average electron and ion temperatures.

Figure 10 shows ion $\langle x \rangle / L$ and x_{rms}/L as a function of t/τ_e for all the simulations with L varied. For all runs the ion center-of-mass is skewed towards the cathode. As noted in the previous section, for a given L, the center-of-mass drifts monotonically towards the cathode in time. At a fixed value of normalized time t/τ_e the ion center-of-mass shifts back towards the center of the two plates as L is increased. So the skewing of the density distribution diminishes as L is increased (for a fixed magnetic field strength). The plot x_{rms}/L shows that the "spread" in ion density is not a strong function of L. This can also be clearly seen in the top plot of Fig. 9. Note also that unlike the center-of-mass, the density spread does seem to asymptote for $t > \tau_e$.

We now consider a series of runs for which only the applied voltage V is varied. All other simulation parameters are the same as in Table I, including the electrode plate separation which is fixed at 1 cm. The top plot of Fig. 11 shows results for normalized total ion charge as a function of time for runs with $V = 0, 50, 100, 200$ V. Note that for the $V = 0$ case, which corresponds directly to the ambipolar diffusion problem considered in Ref. [24], the time dependence of the total charge is not purely exponential at late times. This is due to temperature gradients and temporal variations in both V_M and the temperatures.

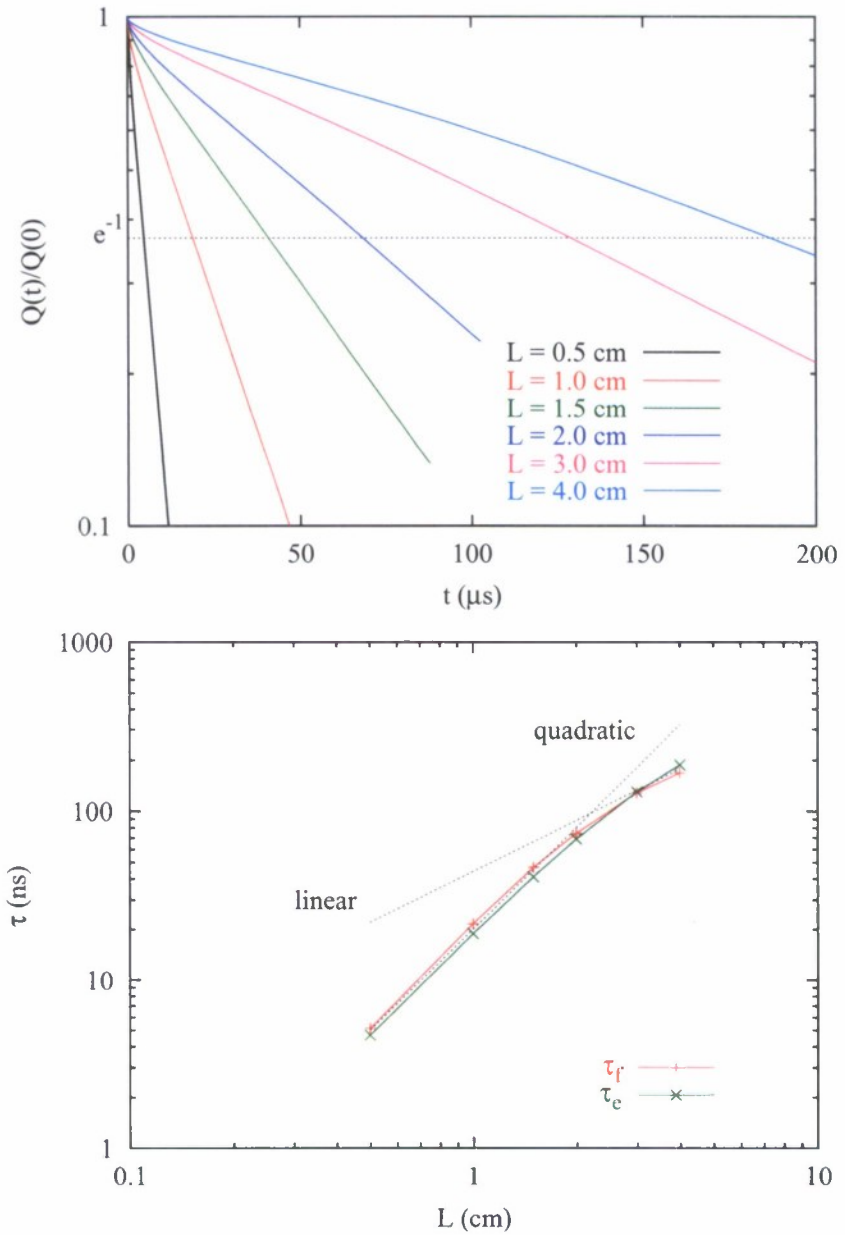

FIG. 8: Results from a series of 1D ReComm simulations. The simulation parameters are the same as those given in Table I, except that the plate separation L is varied. (Top) Normalized total ion charge as a function of time for various values of L. (Bottom) Time scales τ_f and τ_e as a function of L.

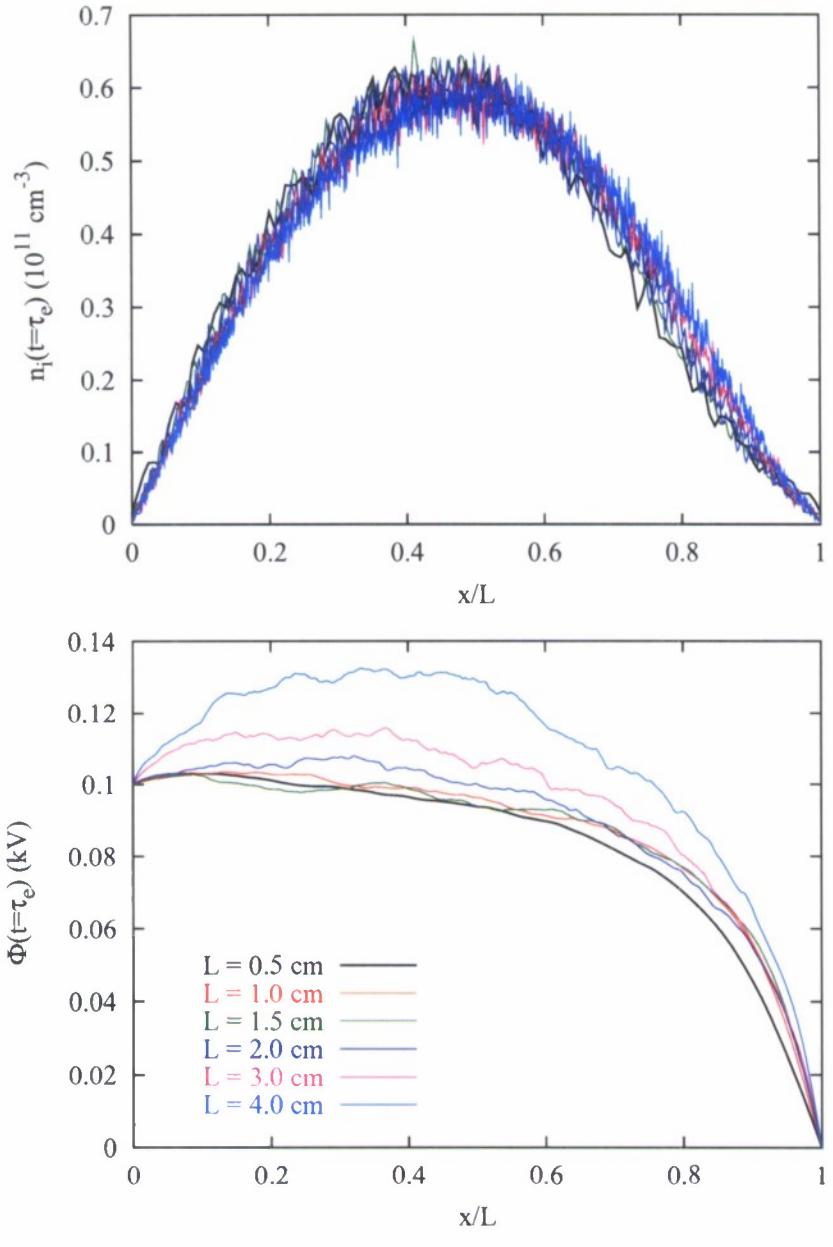

FIG. 9: Results from a series of 1D ReComm simulations. The simulation parameters are the same as those given in Table I, except that the plate separation L is varied. (Top) Normalized ion density at $t = \tau_e$ as a function of x/L. (Bottom) Potential at $t = \tau_e$ as a function of x/L.

For each run, the values of τ_f and τ_e are calculated from the $Q(t)$ data. Of course the value of τ_f for $V = 0$ is a rough estimate by necessity. The inverse values of τ_e and τ_f are plotted as a function of V in the bottom plot of Fig. 11. For $V = 50, 100$, and 200 V, $V_a < 0$

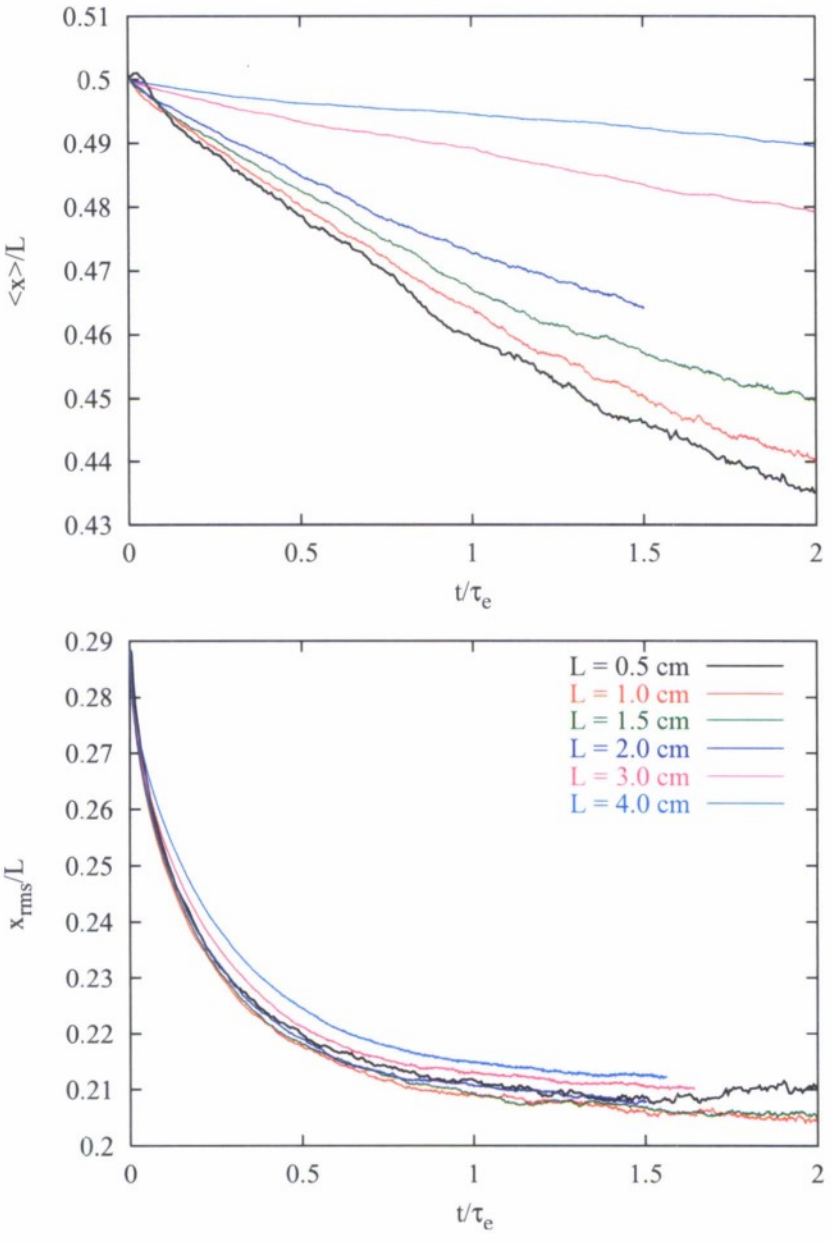

FIG. 10: Results from a series of 1D ReComm simulations. The simulation parameters are the same as those given in Table I, except that the plate separation L is varied. (Top) $\langle x \rangle / L$ as a function of t/τ_e. (Bottom) x_{rms}/L as a function of t/τ_e.

and $V \gg |V_a|$. In this regime, the data suggests that τ is roughly proportional $1/V$. That is, the plasma density can be moved around more quickly as the electrode voltage is increased.

Figure 12 shows the ion density and potential for each simulation as a function of x at

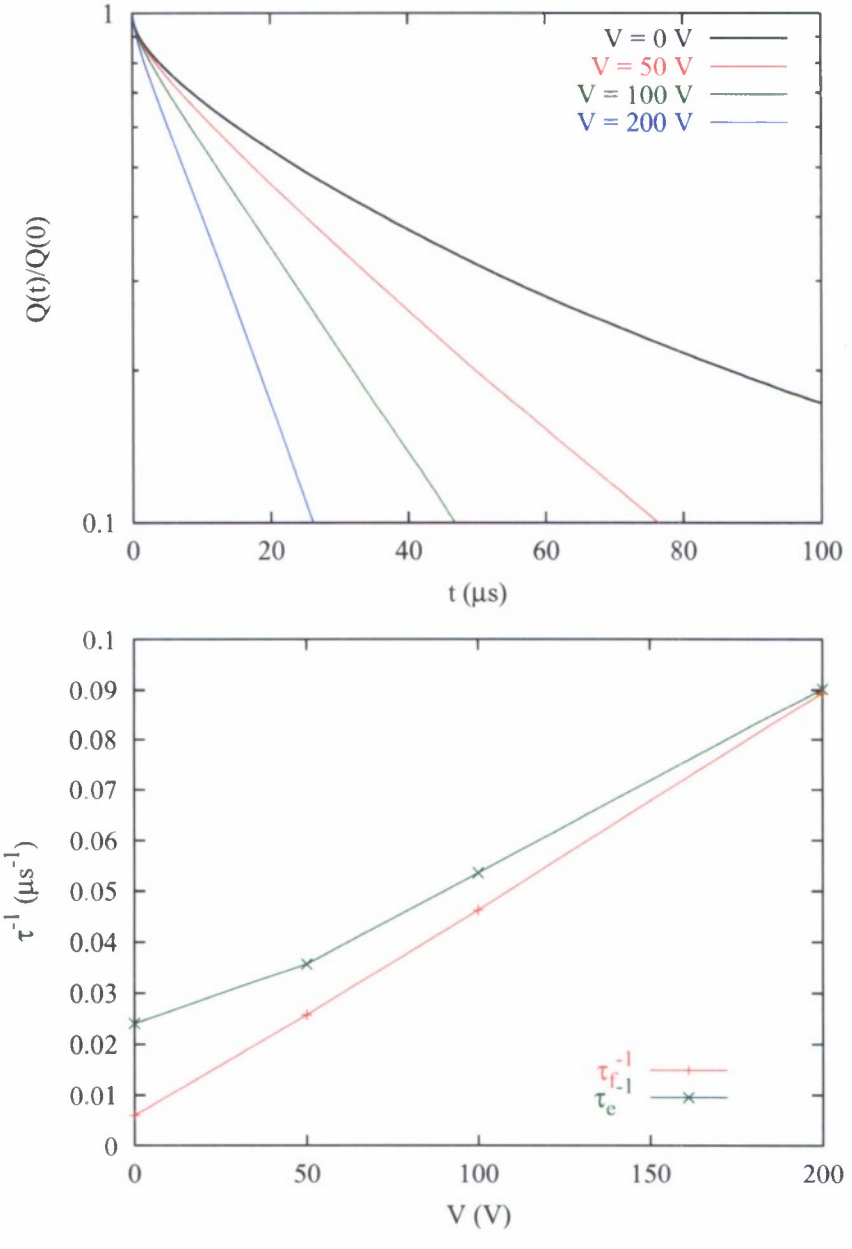

FIG. 11: Results from a series of 1D ReComm simulations. The simulation parameters are the same as those given in Table I, except that the plate voltage V is varied. (Top) Normalized total ion charge as a function of time for various values of V. (Bottom) Time scales τ_f and τ_e as a function of V.

the time $t = \tau_e$. The density profiles again have a nearly self-similar shape, except for the shifting of the ion center-of-mass toward the plate for the runs with an applied voltage. With no applied voltage, the distribution is symmetric about the midpoint between the plates, as is expected by symmetry. If we neglect transients, the position dependence of the temperatures, as well as charge-separation effects, we can roughly estimate that $V_a \sim -2.5$ V and $V_M \sim 10$ V for the run with $V = 0$. For these parameters we can estimate [by solving Eq. (B18)] that $\tau \sim 300$ μs. This is in rough agreement with the measured value of τ_f. For this case ($V = 0$), we note that the mid-potential V_M is of the order of T_e/e which is a few times $-V_a$. The diffusion theory of Ref. [24] predicts an infinite value of V_M for a boundary condition with vanishing plasma density at the electrode surfaces. This does not actually occur as the assumption of quasi-neutrality breaks down near the electrodes and limits the magnitude of V_M. Figure 13 shows the plasma center-of-mass $\langle x \rangle$ and spread x_{rms} for each run as a function of t/τ_e. The temporal drift of the center-of-mass is again evident, except, of course, for $V = 0$ case.

In the next series of runs, the electron-neutral collision frequency ν_{en} is varied from its baseline value of $5\omega_{pi}$. We have performed simulations for $\nu_{en}/\omega_{pi} = 1, 2, 3.5, 5$, and 10. The calculated time constants τ_e and τ_f are plotted as a function of ν_{en}/ω_{pi}. We note that with increasing electron collisionality, the time constants begin to level off. As ν_{en} is increased, the electrons become more and more mobile [for a magnetized plasma species where $\omega_{cs} \gg \nu_{sn}$ the diffusion coefficient and mobility both scale linearly with ν_{sn}; see Eq. (B7)]. In the limit that the electrons become much more mobile than the ions, ambipolar diffusion becomes limited by ion mobility. For this reason $\tau \propto 1/D_a$ asymptotes as seen in Fig. 14.

Figure 15 shows the ion density and potential as a function of x at $t = \tau_e$ for each of the simulations. We note first that for the smaller values of ν_{en}/ω_{pi}, for which the electrons are

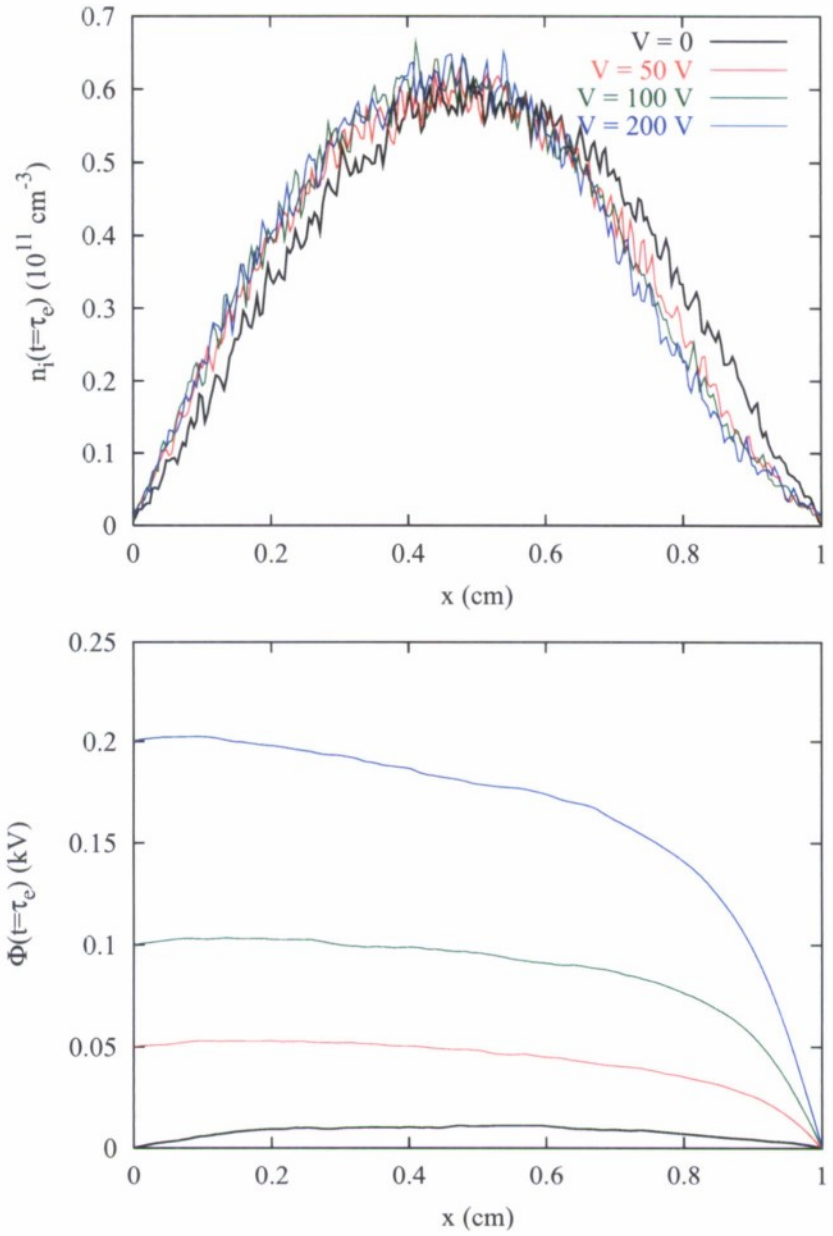

FIG. 12: Results from a series of 1D ReComm simulations. The simulation parameters are the same as those given in Table I, except that the plate voltage V is varied. (Top) Normalized ion density at $t = \tau_e$ as a function of x. (Bottom) Potential at $t = \tau_e$ as a function of x.

relatively less mobile, there large are regions near the cathode completely devoid of ions. Since the electron density is not negligible in this region, there is again a large electrode sheath where charge neutrality breaks down. For these runs the potential plots show that

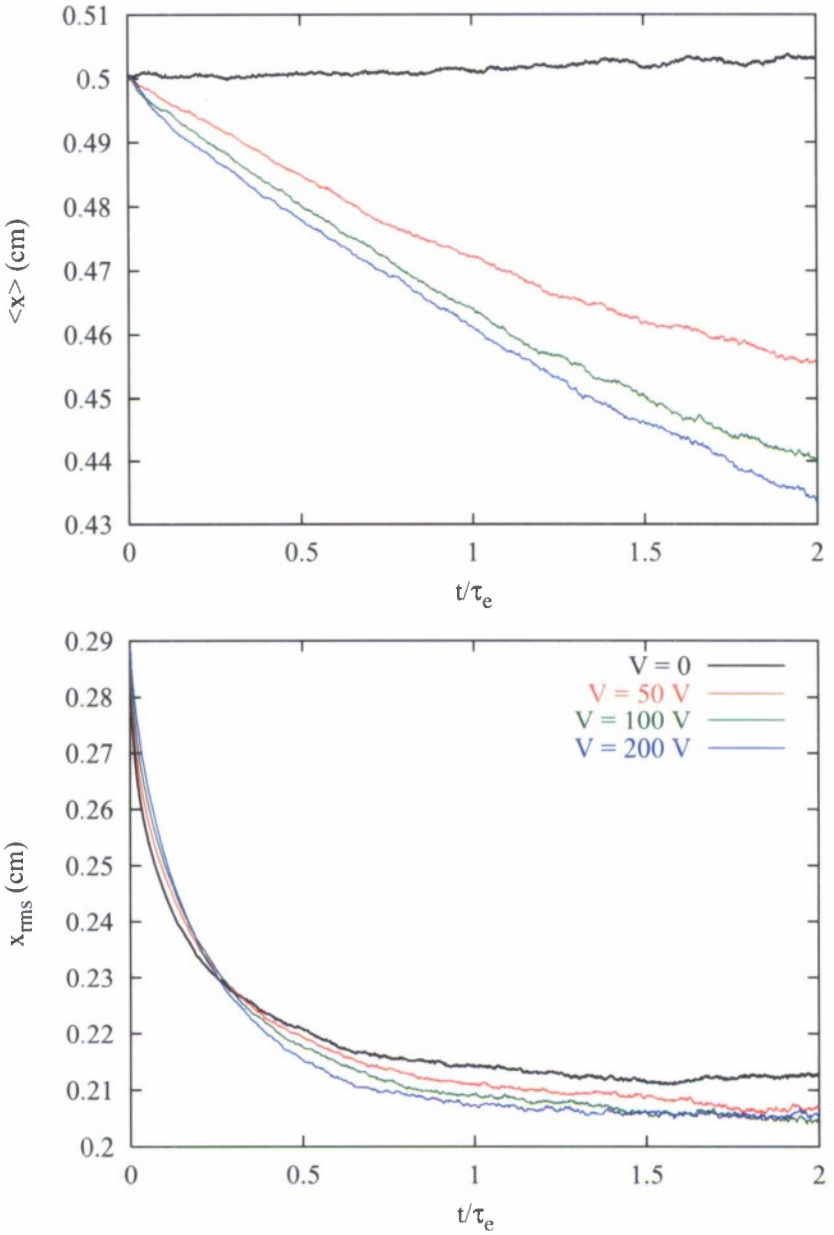

FIG. 13: Results from a series of 1D ReComm simulations. The simulation parameters are the same those as given in Table I, except that the plate voltage V is varied. (Top) $\langle x \rangle$ as a function of t/τ_e. (Bottom) x_{rms} as a function of t/τ_e.

most of the potential is screened out in the region near the cathode, with only a small electric in the remainder of the gap. In the limit that the $\nu_{en} \rightarrow 0$, the electrons are completely immobile, as they are line-tied and can only drift perpendicular to the electrodes. In this

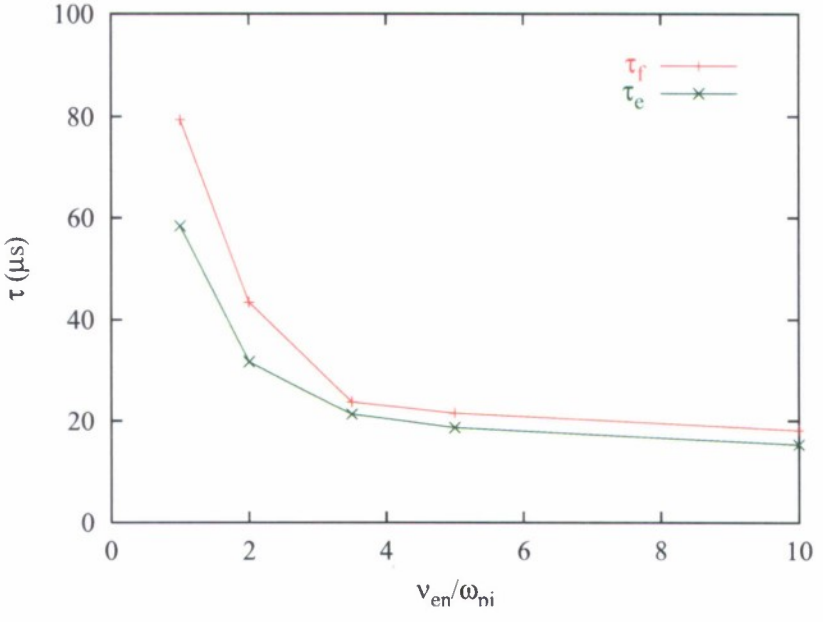

FIG. 14: Timescales τ_f and τ_e are plotted as a function of ν_{en}/ω_{pi}. The simulation parameters are the same as those given in Table I, except that the electron-neutral collision frequency ν_{en} is varied.

case, the potential is completely screened out in a region near the cathode from which ions are excluded. In the remainder of the gap there is no electric field and the ion density distribution remains unaltered. As the electron collision frequency is increased relative to the ions, the large cathode sheath eventually recedes.

Figure 16 shows the ion density center-of-mass and spread as a function of t/τ_e. Note that the center-of-mass shifts towards the anode for low electron collisionality, but shifts back towards the cathode when electron collisionality is increased. This agrees with the general rule, established Appendix B, that the direction of the shift of the center-of-mass is determined by the relative mobility of the two species. When the electrons are more mobile, the density shifts towards the cathode, and when the ions are more mobile the shift is towards the anode.

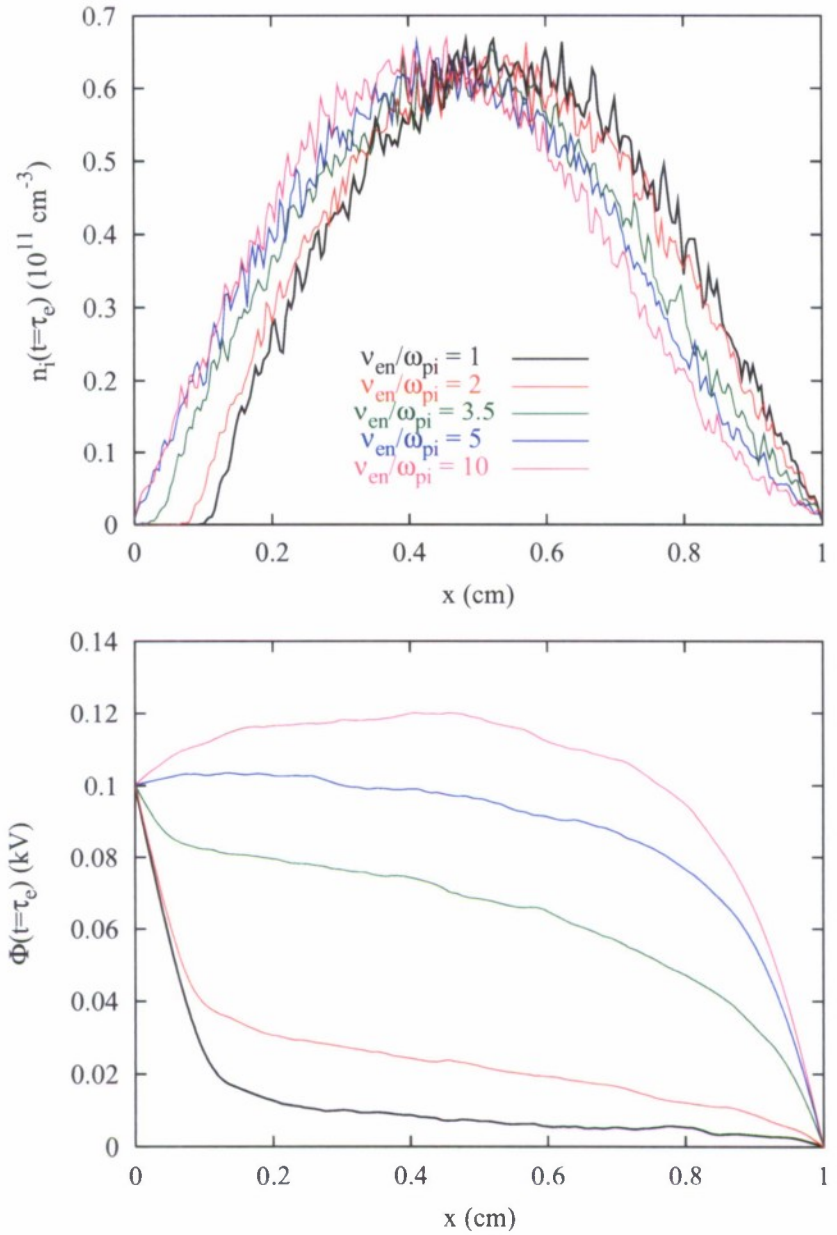

FIG. 15: Results from a series of 1D ReComm simulations. The simulation parameters are the same as those given in Table I, except that the electron-neutral collision frequency ν_{en} is varied. (Top) Normalized ion density at $t = \tau_e$ as a function of x. (Bottom) Potential at $t = \tau_e$ as a function of x.

where

$$\epsilon = 1 - \frac{\omega_{pe}^2}{\omega^2 - \omega_{ce}^2}, \tag{58}$$

and

$$\eta = 1 - \frac{\omega_{pe}^2}{\omega^2}. \tag{59}$$

The Green's function for Eq. (57) is

$$G\left(\vec{r}\right) = \begin{cases} -2\left[|\epsilon\eta|\left(\gamma^2 z^2 - x^2 - y^2\right)\right]^{-1/2}, & |\gamma z| > \sqrt{x^2 + y^2}, \\ 2i\left[|\epsilon\eta|\left(\gamma^2 z^2 - x^2 - y^2\right)\right]^{-1/2}, & |\gamma z| < \sqrt{x^2 + y^2}, \end{cases} \tag{60}$$

where $\gamma^2 = -\epsilon/\eta$.

For the charge density in an antenna defined as

$$\rho(x, y, z) = \frac{I_0}{c}\frac{\cos[\kappa(L - |x|)]}{\sin(\kappa L)}\mathrm{sgn}(x)\delta(y)\delta(z), \tag{61}$$

we can obtain the following expression for the electrostatic potential of oscillations excited by the dipole antenna inside a plasma sheath:

$$\Phi(\vec{r}) = -\frac{2}{|\epsilon\eta|}\int_L^L \frac{\rho(\xi)d\xi}{\sqrt{\gamma^2 z^2 - (x - \xi)^2 - y^2}}. \tag{62}$$

The electrostatic potential defined by Eq. (62) contains resonances surfaces where it has singularities. To find these surfaces and the type of electrostatic potential singularity on these surfaces, we define the function

$$f_1(\xi, x, y, z) = \gamma^2 z^2 - (x - \xi)^2 - y^2. \tag{63}$$

On the resonance surface, the electrostatic potential Φ a logarithmic singularity. This singularity can be identified from the conditions

$$f_1(\xi, x, y, z) = 0, \tag{64}$$

$$\frac{\partial f_1}{\partial \xi} = -2(x - \xi) = 0. \tag{65}$$

These conditions (64)-(65) define parts of the plane

$$\gamma z = \pm y, \tag{66}$$

with $-L < x < L$. Now f_1 can be put into the form

$$f_1(\xi, x, y, z) = \frac{1}{2}\frac{\partial^2 f_1(\xi_s, x_s, y_s, z_s)}{\partial \xi^2}(\xi - xi_s)^2 + \delta f, \tag{67}$$

where

$$\delta f = \left.\frac{\partial f_1}{\partial x}\right|_{x=x_s}(x-x_s)+\left.\frac{\partial f_1}{\partial y}\right|_{y=y_s}(y-y_s)+\left.\frac{\partial f_1}{\partial z}\right|_{z=z_s}(z-z_s) = 2\gamma z_s(z-z_s)-2y_s(y-y_s). \tag{68}$$

With Eq. (67), we can now write the following expression for the potential of the quasi-electrostatic whistler wave in the vicinity of the resonance surface:

$$\Phi_1 = -\frac{2\rho_1}{\sqrt{|\epsilon\eta|}}\int\left[\frac{1}{2}\frac{\partial^2 f_1}{\partial \xi^2}(\xi - xi_0)^2 + \delta f\right]^{-1/2} d\xi. \tag{69}$$

Carrying out the integration in Eq. (69) with $\delta f \neq 0$, we find

$$\Phi_1 = -\frac{i\rho_1}{\sqrt{2|\epsilon\eta|}} \ln\left(\frac{1}{2}\delta f\right) + \text{constant}. \tag{70}$$

From Eq. (70) it is clearly seen that when we are approaching the resonance surface and $\delta f \rightarrow 0$, the potential of the quasi-electrostatic whistler wave experiences a logarithmic singularity. We can use Eq. (70) to find the electric field excited by an antenna in the vicinity of the resonance surface. Introducing the coordinates along and perpendicular to the resonance surface,

$$\chi = \frac{z + \gamma y}{\sqrt{1+\gamma^2}} \quad \text{and} \quad \sigma = \frac{\gamma z - y}{\sqrt{1+\gamma^2}}, \tag{71}$$

we can find that the strongest singularity is experienced by the electric field component directed the normal to the resonance surface. The expression for the electric field has the following form,

$$E_\sigma \simeq 2I_A \frac{\kappa}{\omega\sqrt{|\epsilon\eta|}} \frac{\cos[\kappa(L-|x|)]}{\delta\sqrt{1+\gamma^2}} \text{sgn}(x), \tag{72}$$

where δ is the distance from the resonance surface. From the expression for the excited field, Eq. (72) indicates that the field experiences the $1/\delta$ singularity in the vicinity of the resonance surface. One way to eliminate this singularity is to include the finite plasma temperature into the components of the dielectric tensor. Another possibility is to introduce the finite width of the dipole antenna. Equation (72) is valid at distances from the resonance surface that exceed the electron cyclotron radius or finite antenna width, whatever is larger. This analysis allows us to make an estimate of the wave field excited by the dipole antenna near the resonance surface.

We can estimate the relative importance of different nonlinear processes in vicinity of

the plasma sheath. Using Eq. (72) as an estimate of the electric field excited by the dipole antenna inside the plasma sheath, we estimate the change in the plasma temperature due to the presence of the dipole antenna and, eventually, the level of the random noise produced, which can influence the quality of the communication channel.

The oscillation frequency in the antenna is comparable to the lower hybrid resonance (LHR) frequency, Eq. (55), with characteristic wavelength obtained from $(kc/\omega_{pe})^2 \gg 1$. For the electron density inside the sheath, $n_e \sim 10^{11}$ cm^{-3}, this corresponds to the excited LOR oscillation wavelengths of the order of several centimeters (1 – 3 cm):

$$\lambda \ll \lambda_0 = \frac{2\pi c}{\omega_{pe}} \sim 10 \text{ cm}. \tag{73}$$

For higher plasma densities, these exited wavelengths are smaller. The excited oscillations are known to occur inside the resonance cones oriented along the external magnetic field with an apex angle $\alpha \sim \omega/\omega_{ce}$.

The important parameter which characterizes the nonlinear processes in the vicinity of the antenna is the ratio of the electric field energy to the plasma pressure. For the values of this parameter inside the range:

$$\frac{m}{M} < \frac{E^2}{4\pi n_0 T} < 1. \tag{74}$$

The principal nonlinear effect is wave energy spectrum migration towards smaller wavelengths and the collapse of the lower hybrid waves. This eventually results in resonance absorption of the wave energy by electrons and ions. When the excited filed is stronger and satisfies the condition,

$$\frac{E^2}{4\pi n_0 T} > 1, \tag{75}$$

strong nonlinear effects will be under way. The high radiation pressure will push the plasma out from the resonance cone region and the intersection of the particle trajectories due to the strong parametric instability will heat the plasma as a whole. Taking the current in antenna $I_A \sim 3$ to 4 A, and using the plasma parameters and magnetic field strength presented above, we can use Eqs. (72) and (75) to show that the LOR oscillations in the vicinity of the antenna are unstable.

B. Plasma heating by quasi-electrostatic whistler waves in the vicinity of a VLF antenna inside a plasma sheath

Assuming that the wavelength of the excited waves is on the order of the thickness of a plasma sheath, we examine the nonlinear interaction of the pump field,

$$\vec{E}_0(t) = \vec{E}_0 \sin(\omega_0 t), \tag{76}$$

with the plasma sheath. We are interested in the case when the waves excited by the antenna field is strong enough to satisfy condition (75), indicating the presence of strongly nonlinear coupling effects. The high radiation pressure will push out the plasma from the resonance cone region and the intersection of particle trajectories due to a strong parametric instability will heat the plasma as a whole. The instability of the plasma in the external electric and magnetic fields due to excitation of electrostatic oscillations near the lower hybrid resonance was investigated in a series of papers. The dispersion equation for parametric instability for the case when the oscillation speed of electrons in the external electric field is small in comparison with the thermal velocity, including the influence of Coulomb collisions, was derived by Andreev and Kirii [25]. Nonresonant decay neglecting the thermal motion of

particles, which is possible in a strong electric field of the pump wave when the energy of oscillations of electrons is sufficiently larger than their thermal energy, is examined by Porkolab [26]. The experimental observation of parametric instability in the range of frequencies we are interested in and with the frequency of the pump wave $\omega_0 \leq 3\omega_{LH}$ was presented by Bonizzoni *et al.* [27], where it was noticed that the excitation of a broad spectrum of non-resonant quasi-ion modes takes place. This is also the situation in our case, but now with a very strong pump wave, when the condition (75) is satisfied and forced oscillations with the growth rate γ (for $\omega_{ci} \ll \gamma < \omega_{LH}$) are excited. Contrary to the case considered by Bonizzoni *et al.*, we ignore the dispersive effects due to the thermal motion of plasma particles.

C. Dispersion Equation for Parametric Instability

We present a brief derivation of a dispersion equation which describes the parametric excitation of lower oblique resonance oscillations in the presence of strong pump wave with the frequency $\omega_0 > \omega_{LH}$. We consider the pump field homogeneous in space, with temporal profile given by Eq. (76). As mentioned above, the wavelengths under consideration are short in comparison with the characteristic scale length of the inhomogeneity of the field of the pump wave. Taking into account that the wavelength of the quasi-electrostatic whistler waves excited by the VLF antenna are $\lambda \sim 2\pi c/\omega_{pe}$, giving $k \gg \omega_{pe}/c$. We analyze nonlinear excitation of quasi-electrostatic oscillations with the frequencies above the lower hybrid frequency due to a presence of the pump field produced by a VLF antenna. Below, n_e and n_i are the electron and ion density perturbations in the excited oscillations and $\vec{V}_e$ and $\vec{V}_i$ are the velocity perturbations. Furthermore, δn_e and δn_i as well as δV_e and δV_i are the perturbations parametrically connected to the low frequency plasma dynamics.

For the electron speed at high frequency one can write:

$$V_{ex} = \frac{e}{m\omega_{ce}} E_y - \frac{e}{m\omega_{ce}^2} \left(\frac{\partial}{\partial t} + i\vec{k}\vec{U}_{0e} \right) E_x, \tag{77}$$

and

$$V_{ey} = -\frac{e}{m\omega_{ce}} E_x - \frac{e}{m\omega_{ce}^2} \left(\frac{\partial}{\partial t} + i\vec{k}\vec{U}_{0e} \right) E_y. \tag{78}$$

In Eqs. (77) and (78), $\vec{E} = \vec{E}(t)\exp(i\vec{k}\vec{r})$ is the parametrically excited field of oscillations. The electron speeds due to the pump wave are defined as

$$\vec{U}_{0e} = \frac{e}{m\omega_{ce}} \left(E_{0y}\hat{e}_x - E_{0x}\hat{e}_y \right) \sin\left(\omega_0 t\right). \tag{79}$$

Now we can write expressions for the perturbations of the electron and ion densities due to the high frequency oscillations, using the continuity and Poisson equations,

$$\left(\frac{\partial}{\partial t} + i\vec{k}\vec{U}_{0e} \right)^2 n_e + \frac{\omega_{pe}^2}{1+\omega_{pe}^2/\omega_{ce}^2} \frac{k_z^2}{k^2} n_e = \frac{1}{1+\omega_{pe}^2/\omega_{ce}^2} \left(\frac{\partial}{\partial t} + i\vec{k}\vec{U}_{0e} \right)^2 n_i + \tag{80}$$

$$\frac{c}{B_0} \frac{1}{1+\omega_{pe}^2/\omega_{ce}^2} \left(\frac{\partial}{\partial t} + i\vec{k}\vec{U}_{0e} \right) \left\{ \left[\vec{E}_{0\perp} \times \vec{\nabla}\delta n \right]_z + \frac{\omega_{ce}}{\omega_0} \left[E_{0z} \cos\left(\omega_0 t\right) \right] \frac{\partial \delta n}{\partial z} \right\},$$

$$\left(\frac{\partial}{\partial t} + i\vec{k}\vec{U}_{0i} \right)^2 n_i = \omega_{pi}^2 \left(n_e - n_i \right). \tag{81}$$

In Eq. (81), the expression

$$\vec{U}_{0i} = -\frac{e\vec{E}_0}{M\omega_0} \cos\left(\omega_0 t\right)$$

is the oscillatory speed of the ions in the pump wave field. We now introduce the function

$$\eta_e(t) = n_e \exp\left(-i\vec{k}\vec{a}_e \right), \tag{82}$$

which corresponds to the electron charge density in the coordinate frame oscillating together with the electrons under the action of the pump field. In Eq. (82), for $\vec{a}_e$ we have

$$\vec{a}_e(t) = -\frac{e}{m\omega_{ce}\omega_0}\left(E_{0y}\hat{e}_x - E_{0x}\hat{e}_y\right)\cos\left(\omega_0 t\right) + \frac{e}{m\omega_0^2}E_{0z}\sin\left(\omega_0 t\right)\hat{e}_z. \tag{83}$$

For the ions, we consider

$$\frac{\partial}{\partial t} \gg \vec{k}\vec{U}_{0i}.$$

After averaging over the fast time $\sim \omega_0^{-1}$, we obtain

$$\left(1+\frac{\omega_{pe}^2}{\omega_{ce}^2}\right)\frac{\partial^2\eta_e}{\partial t^2} + \omega_{pe}^2\frac{k_z^2}{k^2} = \frac{\omega_{pe}^2}{\omega_{ce}^2}J_0\left(b_3\right)\frac{\partial^2 n_i}{\partial t^2} + \omega_{pe}^2 J_0\left(b_3\right)\left[\frac{k_z^2}{k^2} - \frac{1}{2}\frac{\omega_0^2}{\omega_{ce}^2}b_3^2\right]n_i + \tag{84}$$

$$\frac{c}{B_0}J_0\left(b_3\right)\frac{\partial}{\partial t}\left\{\left[\vec{E}_{0\perp}\times\vec{\nabla}\delta n\right]_z + \frac{\omega_{ce}}{\omega_0}E_0\cos\left(\omega_0 t\right)\frac{\partial\delta n}{\partial z},\right\}$$

$$\left(\frac{\partial^2}{\partial t^2}+\omega_{pi}^2\right)n_i = \omega_{pi}^2 J_0(b)v_e, \tag{85}$$

where for b_3 we have

$$b_3 = \frac{e}{m\omega_0^2}\sqrt{\frac{\omega_0^2}{\omega_{ce}^2}\left[\vec{E}_0\times\vec{k}\right]_z^2 + k_z^2E_{0z}^2}, \tag{86}$$

and J_0 is the zeroth-order Bessel function.

Assuming the following characteristic frequency range

$$kV_{Ti} \ll \Omega \ll k_z V_{Te}, \tag{87}$$

where V_{Te} and V_{Ti} are the electron and ion thermal velocities, we derive an expression for the low frequency ion acoustic oscillation. Assuming that the electrons are magnetized, the

low frequency electron oscillations can be described by the following equation of motion,

$$e\frac{\partial}{\partial z}\delta\Psi = m\frac{V_{Te}^2}{n_0}\frac{\partial \delta n_e}{\partial z} + m\left\langle\left(V_e\vec{\nabla}\right)V_{ez}\right\rangle, \tag{88}$$

where the electron inertia term is omitted and $\delta\Psi$ is the electrostatic potential of the parametrically excited ion acoustic oscillations, and the angle brackets around the last term indicate averaging over the fast time scale ω_0^{-1}. The Poisson equation for Ψ is

$$\Delta\Psi = 4\pi e\left(\delta n_e - \delta n_i\right), \tag{89}$$

where Δ is the Laplacian operator.

Noting that the ion motion is unmagnetized, we obtain the following nonlinear differential equation for the density perturbations in the low frequency oscillations,

$$\left[\frac{\partial^2}{\partial t^2} + \left(\vec{U}_{0i}\dot{\vec{n}}abla\right)^2 - V_s^2\Delta\right]\frac{\partial\delta n}{\partial z} = n_0\frac{m_i}{M}\Delta\left\langle\left(\vec{V}_e\Delta\right)V_{ez}\right\rangle, \tag{90}$$

where V_s is the sound speed.

We can now use Eqs. (83), (84), and (88) to obtain the dispersion relation for the parametric instability of the oblique resonance oscillations. First, using a standard procedure, we introduce two high frequency oscillations nonlinearly excited by the parametric instability with frequencies ω_1 and ω_2 and a low frequency ion-acoustic perturbation at frequency Ω,

$$\eta_{e1} = A_{1k}\exp\left[i\left(\vec{k}\vec{r} - \omega_1 t\right)\right], \qquad n_{i1} = B_{1k}\exp\left[i\left(\vec{k}\vec{r} - \omega_1 t\right)\right], \tag{91}$$

$$\eta_{e2} = A_{2k}\exp\left[-i\left(\vec{k}\vec{r} + \omega_2 t\right)\right], \qquad n_{i2} = B_{1k}\exp\left[-i\left(\vec{k}\vec{r} + \omega_2 t\right)\right], \tag{92}$$

$$\delta n = \delta n_k \exp\left[i\left(\vec{k}\vec{r} - \Omega t\right)\right]. \tag{93}$$

Next we substitute Eqs. (91)-(93) into Eqs. (84), (85), and (90) to obtain the dispersion relation for simultaneous parametric excitation of two high frequency oscillations with frequencies given by

$$\omega_{1,2}^2 = \frac{\omega_{pi}^2}{1+\omega_{pe}^2/\omega_{ce}^2}\left\{1 + \frac{\omega_{pe}^2}{\omega_{ce}^2}\left[1 - J_0^2\left(b_3\right)\right] + \frac{M}{m}\frac{k_z^2}{k_2}\right\}, \tag{94}$$

and a low-frequency ion-acoustic frequency perturbation. The dispersion relation has the following form

$$\Omega^2 + \frac{1}{2}k^2 a_i^2 \omega_0^2 - k^2 V_s^2 = \frac{1}{4}\frac{e^2}{m^2}\frac{\omega_{LH}^2}{\omega_{ce}^2}\frac{1}{\omega_1}J_0^2(b)\left[\vec{k}\times\vec{E}_0\right]_z^2 \frac{\delta}{\delta^2 - \Omega^2}, \tag{95}$$

where $\delta = \omega_0 - \omega_1$ and $a_i = e^2 E_0^2/M^2\omega_0^4$.

It is necessary to point out that we are interested in the supersonic regime of parametric instability excitation, i.e. when

$$\Omega \gg kV_s. \tag{96}$$

$\omega_0 - \omega_1 < 0$, Aperiodic Instability

For $\delta < 0$, aperiodic instability takes place with a peak growth rate of

$$\gamma_{max,aper} \simeq \omega_{LH}\left[\frac{1}{4}\frac{M}{m}\frac{\omega_{pe}^2}{\omega_{ce}^2}J_0^2(b)\frac{E_0^2}{4\pi m n_0 c^2}\right]^{1/3}. \tag{97}$$

To determine the plasma temperature, we take into account that the effective electron collision frequency is of the order of the instability growth rate, $\nu_{eff} \sim \gamma$. In the vicinity of the heated plasma, condition (92) holds, and electrons drift along the magnetic field lines with sound speed C_s. Here the energy balance can be expressed as

$$C_s \frac{\partial}{\partial t}(nT) = \left(1 + \frac{\omega_{pe}^2}{\omega_{ce}^2}\right) \nu_{eff} \frac{\left|\vec{E}_0\right|^2}{8\pi}. \tag{98}$$

Substituting Eq. (97) into Eq. (98), the following estimate of an effective plasma temperature increase in the heated region can be obtained,

$$T \sim \left(\frac{1}{2}\omega_{pi} L \sqrt{M} mc^2\right)^{2/3} \left(\frac{M}{m}\right)^{1/9} \left(\frac{\left|\vec{E}_0\right|^2}{4\pi mnc^2}\right)^{8/9}, \tag{99}$$

where L is the characteristic length of the heated region.

$\omega_0 - \omega_1 > 0$, Periodic Instability

For $\delta > 0$, the temperature enhancement can be found analogously. The dispersion relation now takes the form

$$\Omega^2 + \frac{1}{2}k^2 a_i^2 \omega_0^2 - k^2 C_s^2 = \frac{1}{4}\frac{e^2}{m^2}\frac{\omega_{LH}^2}{\omega_{ce}^2}\frac{1}{\omega_1} J_0^2(b) \left[\vec{k} \times \vec{E}_0\right]_z^2 \frac{\delta}{\delta^2 - \Omega^2}. \tag{100}$$

For $\delta > 0$, periodic instability occurs with a peak growth rate

$$\gamma_{max,per} \simeq \frac{\sqrt{3}}{2}\omega_{LH} \left[\frac{1}{16}\frac{M}{m}\frac{\omega_{pe}^2}{\omega_{ce}^2} J_0^2(b) \frac{E_0^2}{4\pi m n_0 c^2}\right]^{1/3}. \tag{101}$$

The peak growth rate of the parametric instability can be written in the form

$$\gamma_{max} \sim (ka_e)^{3/2} \omega_{LH}, \tag{102}$$

where $k \sim \omega_{pe}/c$ and a_e is the displacement of an electron during the period of oscillations due to the drift in the wave field.

After the same sequence of substitutions as in the case of periodic instability, the rise in plasma temperature is found to be

$$T \sim \left(\frac{1}{4}\omega_{LH} L\sqrt{M} mc^2\right)^{2/3} \left(\frac{\omega_{pe}^4}{\omega_{ce}^4}\right)^{5/9} \left(\frac{M}{m}\right)^{2/9} \left(\frac{\left|\vec{E}_0\right|^2}{4\pi mnc^2}\right)^{8/9}. \tag{103}$$

Equations (99) and (103) are similar in form and predict similar temperature increases.

As an example, we consider a current running in the antenna $I_0 \sim 1$ A, the plasma density inside the sheath of 10^{11} cm^{-3}, and external magnetic field of 1 T. We can estimate the field excited in the vicinity of the antenna to be $E_0 \sim 0.6$ statvolt/cm. From Eq. (103) we can estimate the increase in plasma temperature due to the presence of the electric field excited by the antenna to be $T \sim 7$ eV. This rough estimate confirms that indeed the plasma in the vicinity of the VLF antenna can undergo a significant increase in temperature. This in turn can strongly influence the dielectric properties of the plasma and lead to enhanced disturbance of the received signals.

V. DISCUSSION AND SUMMARY

The analysis of the conversion between EM and EAWs has been carried out for a sharp plasma boundary, and the results demonstrate reasonable power for the transmitted EM

waves. Our next step is to evaluate the feasibility of carrying out EM PIC simulations to model the generation and propagation of the EAWs and their transformation to EM waves at the plasma-vacuum interface.

In a separate report [12], we expanded on our previous analysis of the magnetic window analysis, adding revised 2D PIC simulations and new 3D PIC simulations of the wave propagating in a microwave horn and the interaction with a plasma layer.

Our initial analysis of the ReComm scheme [18, 28, 29], where applied electric and magnetic fields are used to open a frequency-space window for EM wave propagation through the plasma sheath, is presented in Sec. III. We have established that the ion distribution in the cross-field dipole (in the plasma-optic regime) is altered significantly only on diffusion time scales, for which $\tau \propto L^{\gamma}/V$, where $\gamma \sim 1-2$. For plasma parameters believed to be consistent with the radio blackout regime, τ is of the order of tens of μs, when L on the order of a few cm, and V is on the order of 100 V. For a realistic ReComm device allowing communication in the L-band of the radio spectrum, the diode length L would have to be scaled up to something on the order of 1 m. The magnitude of the applied voltage V is, of course, limited by practical considerations. The utility of the ReComm scheme depends upon being able to alter the plasma density profile on a timescale which is short compared to the time it takes the hypersonically flowing plasma to pass by the diode. So it questionable whether τ can be made small enough to be useful in alleviating the blackout problem. As mentioned above, scaling the electrode separation up to lengths of 1 m would require dropping the magnetic field strength to remain in the plasma optic regime. This will alter the magnetization (ratio of cyclotron and collision frequencies) of the plasma species and could alter the scaling at longer diode lengths.

We have shown that an ambipolar diffusion theory of the cross-field diode can describe

qualitatively the results of the simulation. However, plasma energy transport and charge separation effects, neglected in the theory, play an important role in determining the details of the plasma evolution. We have shown in our baseline simulation that ion temperatures can reach values of several tens of eV on long time scales $t \sim \tau$. This suggests that Ohmic heating of the plasma may lead to further ionization. To examine such effects would require replacing the simple Drude collision model used in this report with a more realistic chemistry model. Although it is probably more important to establish initially that τ can be made small enough for practical use.

Another concern is that the direction in which the plasma is shifted by the applied field depends sensitively on the relative mobility of the electrons and ions. To determine the relative mobility, it is necessary to have reliable information about the electron and ion temperatures and collision frequencies in the sheath surrounding the vehicle. Our survey of the literature suggests that the existence of this information is still incomplete.

We note that the ReComm scheme is based only on altering the local plasma density in the vicinity of the antenna. To do this requires both an applied magnetic field and a high voltage diode. Moreover the effect may occur only on prohibitively long time scales. By contrast the magnetic window approach [30], which utilizes the magnet but does not require the diode, does not require any slow bulk motion of the plasma, but instead alters the transparency of the existing plasma to the RF signal. But the effectiveness of this alternate scheme depends strongly on the plasma collisionality [12], which, as noted above, is not well known.

In all communication scenarios under consideration, the computational models will be extended to include, with increasing levels of complexity, realistic gas and plasma properties associated with hypersonic flight [31–33]. The goal of this integrated theoretical analysis is

the formulation of "operational-windows" in which physical constraints associated with each communication scheme can be parameterized. This analysis should significantly impact the down-select of these schemes for eventual deployment on hypersonic vehicles.

Acknowledgments

The authors thank Mr. C. Mostrom, Voss Scientific, for assistance with all of the simulations and data analysis presented here, and Mrs. M. Dyson, Voss Scientific, for assistance with the preparation of this report. We thank Dr. Arje Nachman, AFOSR/NE, and Dr. Charles Jones, AFOSR, for technical discussions related to this project and Ms. Valerie Valdez, Technical Information Specialist at the DTIC Southwest Office, for expert assistance in obtaining technical reports and other research documents. Dr. V. Sotnikov acknowledges Dr. James Ernstmeyer and Dr. Saba Mudaliar for helpful discussions. This work was supported by the AFOSR through contract number FA9550-07-C-0049.

APPENDIX A: NUMERICAL CALCULATION OF THE TRANSFORMATION COEFFICIENT

The following C computer program was developed by Dr. Vladimir Sotnikov to numerically calculate the wave transformation coefficient. Electronic copies of the program can be obtained directly from Dr. Sotnikov (sotnikov@unr.edu).

```
/*************************************************/
/*      03-16-08                                 */
/*                                               */
/*     EAW_TR                                    */
/*     Electron Acoustic wave transformation     */
/*                                               */
/*     this program creates the data array output  */
```

```
    /*     with 2 columns (theta3, WT). theta3 is the  */
    /*     propagation angle of the outgoing EM wave.  */
    /*     WT is the coefficient of transformation     */
    /*     calculated as the ratio of energy fluxes    */
    /*     (Pointing vectors) of outgoing EM wave to   */
    /*     the incident EAW. Description is in reports */
    /*     for January, February and March 2008.       */
    /*                                                 */
    /*                                                 */
    /*************************************************/

    #include <iostream.h>
    #include <stdio.h>
    #include <math.h>

    main()
    {
            int   i;
            float Tec, Teh, nec, neh;
            float omega, omegapec, omegapeh;
            float omega2, omegapec2, omegapeh2;
            float c, pi, VTec, VTeh, lambdas;
            float absepsc, absepstot, G;
            float rDec, rDec2, rDeh, rDeh2, RD, RD2;
            float a1,a2,a3, invrDc2, invrDh2, delta, q1;
            float invrDec2, invrDeh2, invrDeh;
    /*************************************/

            Tec = 0.2;
            Teh = 20.0;
            nec = 0.86e11;
            neh = 0.05e11;
            pi = 3.14;
            c = 3e10;
            VTec = 4.19e7*sqrt(Tec);
            VTeh = 4.19e7*sqrt(Teh);
            omegapec = 5.64e4*sqrt(nec);
            omegapec2 = omegapec*omegapec;
            omega = 0.1*omegapec;
            omega2 = omega*omega;
            omegapeh = 5.64e4*sqrt(neh);
            omegapeh2 = omegapeh*omegapeh;
```

```
        rDec = VTec/omegapec;
        rDeh = VTeh/omegapeh;
        rDeh2 =rDeh*rDeh;
        rDec2 = rDec*rDec;
        invrDeh = 1.0/rDeh;
        cout << invrDeh;
        invrDec2 = 1.0/rDec2;
        invrDeh2 = 1.0/rDeh2;
        RD2 = (rDec2*rDeh2)/(rDec2+rDeh2);
        //aa = sqrt(omegapec2/omega2);
        q1 = invrDeh*(1.0/sqrt((omegapec2/omega2)-1.0));
        //q1 = invrDeh*(1.0/sqrt((omegapec2/omega2)));
        lambdas = (2*pi)/q1;
        //lambdas = 1.0;
        cout << lambdas;
        a1 = VTeh/c;
        a2 = omegapec/omegapeh;
        a3 = omega/(c*q1);
        absepsc = (omegapec2/omega2)-1.0;
        G = 1.0+(RD2/rDeh2)*(1.0/absepsc);
        absepstot = ((omegapec2+omegapeh2)/omega2) - 1.0;

/*******************************************/

        FILE *fw;

                fw = fopen("plasma_parameters.dat", "w");

                fprintf(fw, "%f %f %f \n", omegapec, omegapeh, omega);
                fprintf(fw, "%f %f %f %f \n", VTec, VTeh, absepstot, q1);

        fclose(fw);
/*******************************************/

        float theta3[201];
        float WT[201];
        float aa[201];
        float bb[201];
        float cc[201];
        float dd[201];

        delta = (pi/2.0)/200.0 ;
```

```
/*****************************************/

                FILE *fw1;

                fw1 = fopen("WT.dat", "w");

/*********************************************/

        for ( i = 0; i <= 200; i++ )
        {
                theta3[i] = delta*i;
                aa[i] =
16.0*pi*absepsc*a1*a2*cos(theta3[i])*sin(theta3[i])*sin(theta3[i]);
                bb[i] =
(a3/G)*sin(theta3[i])*sin(theta3[i])-absepstot*cos(theta3[i]);
                dd[i] = bb[i]*bb[i];
                cc[i] = absepsc + sin(theta3[i])*sin(theta3[i]);
        WT[i] = aa[i]/(dd[i]+cc[i]) ;

//WT[i] = (16.0*pi*absepsc*a1*a2*cos(theta3[i])*sin(theta3[i])*sin(theta3[i]))/
//
(((a3/G)*sin(theta3[i])*sin(theta3[i])-absepstot*cos(theta3[i]))*
//              ((a3/G)*sin(theta3[i])*sin(theta3[i])-absepstot*cos(theta3[i]))
+
//              (absepsc + sin(theta3[i])*sin(theta3[i]))) ;


fprintf(fw1, "%d %f %f %f %f %f \n", i, theta3[i], WT[i]);
        }

/*************************************************/

        fclose(fw1);
}
```

APPENDIX B: AMBIPOLAR DIFFUSION IN A CROSSED-FIELD DIODE

We review the problem of ambipolar diffusion in a slab, which is treated in some detail in Ref. [24] (see pp 157-163 of the reference). We expand the treatment to allow for the application of an applied voltage across the electrode plates containing the plasma.

The ambipolar diffusion equation comes from considering continuity and momentum equations for both ions and electrons in which quasi-neutrality is assumed to hold, that is, $n_e \simeq n_i$. As with the simulations, we assume that collisionality for each plasma species is dominated by neutrals, and represented by a constant collision frequency ν_{sn}, where $s = i$ or e, for ions and electrons, respectively. We also assume constant plasma temperatures. If the convective derivative in the momentum equations can be neglected, an Ohm's law expression results

$$\mathbf{v_s} = \pm\mu_s \mathbf{E} - D_s \nabla(\ln n), \tag{B1}$$

where n is the quasi-neutral plasma density. The top(bottom) sign in Eq. (B1) applies to ions(electrons). The mobility of species s is defined as

$$\mu_s = \frac{e}{m_s \nu_{sn}}, \tag{B2}$$

where we have assumed $Z = 1$ for all ions, and the diffusion coefficient is given by

$$D_s = \frac{T_s}{m_s \nu_{sn}}. \tag{B3}$$

To maintain quasi-neutrality, it is necessary to equate electron and ion fluxes, $n\mathbf{v_i} = n\mathbf{v_e}$. From this we obtain the ambipolar electric field

$$\mathbf{E} = V_a \nabla(\ln n), \tag{B4}$$

where V_a has dimensions of voltage, and is given by

$$V_a = \frac{D_i - D_e}{\mu_i + \mu_e}. \tag{B5}$$

Note that the sign of V_a depends on the relative magnitudes of the electron and ion diffusion coefficient magnitudes. When $V_a < 0$, electrons are the more "mobile" species and the ambipolar field adjusts to slow down the electrons so that their flux remains equal to that of the less mobile ions. When $V_a > 0$, the ions are the more mobile species.

Inserting the common flux into either the ion or electron continuity equation results in a diffusion equation with the ambipolar diffusion coefficient

$$D_a = \frac{\mu_i D_e + \mu_e D_i}{\mu_i + \mu_e}. \tag{B6}$$

Equations (B2) and (B3) were derived for an unmagnetized plasma. As shown in Ref. [24] (pp 169-173), for diffusion perpendicular to the magnetic field the mobility and diffusion coefficients for each species are easily modified:

$$\begin{aligned} \mu_s &= \frac{e}{m_s \nu_{sn}} \frac{1}{1 + (\omega_{cs}/\nu_{sn})^2}, \\ D_s &= \frac{T_s}{m_s \nu_{sn}} \frac{1}{1 + (\omega_{cs}/\nu_{sn})^2}. \end{aligned} \tag{B7}$$

The expressions for the ambipolar voltage V_a and diffusion coefficient D_a *across* field lines are still given by Eqs. (B5) and (B6), as long as μ_s and D_s are calculated by Eq. (B7).

For the parameters in Table I, ω_{ce}/ν_{en} and ν_{in}/ω_{ci} are both much greater than one. In this regime

$$V_a \sim \left(\frac{T_i}{e}\frac{\omega_{ce}}{\nu_{en}} - \frac{T_e}{e}\frac{\nu_{in}}{\omega_{ci}}\right)\left(\frac{\omega_{ce}}{\nu_{en}} + \frac{\nu_{in}}{\omega_{ci}}\right)^{-1},$$
$$D_a \sim \frac{T_e + T_i}{m_e \omega_{ce}}\left(\frac{\omega_{ce}}{\nu_{en}} + \frac{\nu_{in}}{\omega_{ci}}\right)^{-1}. \tag{B8}$$

Actually, for the parameters in Table I, ω_{ce}/ν_{en} and ν_{in}/ω_{ci} only differ by about 25%. In this case, using the initial plasma temperatures, we can make the simple approximation $eV_a \sim -T_e/2 \ -5$ eV. Since $V_a < 0$, it follows from Eq. (B5), that $D_e > D_i$, or that the electrons are the more mobile of the two species.

We now look for a solution of the ambipolar diffusion equation in one dimension ($\partial/\partial y = \partial/\partial z = 0$). We consider the problem of a plasma confined between two conducting plates of large extent. Namely a cathode at $x = 0$, and an anode at $x = L$. For electrodes with length and width comparable to the plate separation L, it is important to consider diffusion both parallel and perpendicular to the magnetic field. But we neglect these multi-dimensional effects for the present.

We follow the treatment of Ref. [24] and search for a solution by separation of variables

$$n(x,t) = e^{-t/\tau} S(x). \tag{B9}$$

The diffusion equation is satisfied when $S(x)$ is any linear combination of $\cos(kx)$ and $\sin(kx)$ consistent with the boundary conditions of the problem, where

$$k^2 = 1/(D_a\tau). \tag{B10}$$

Integrating Eq. (B4) from the cathode surface at $x = 0$ to an arbitrary field point x yields the electrostatic potential

$$\Phi(x) - \Phi(0) = -V_a \ln[S(x)/S(0)]. \tag{B11}$$

The applied voltage difference V is given by

$$V = \Phi(0) - \Phi(L). \tag{B12}$$

We also define the mid-potential V_M as the voltage difference between the center and the cathode,

$$V_M = \Phi(L/2) - \Phi(0). \tag{B13}$$

If we choose $\Phi(L) = 0$, $V_M = \Phi(L/2) - V$. From Eqs. (B11), (B12) we find

$$\frac{S_A}{S_K} = e^{V/V_a}, \tag{B14}$$

where $S_K = S(0)$ and $S_A = S(L)$. This equation constitutes a boundary condition on the solution for $S(x)$. We can also show [Eqs. (B11) and (B13)] that

$$\frac{S_K}{S_M} = e^{V_M/V_a}, \tag{B15}$$

where $S_M = S(L/2)$. A general solution for $S(x)$ can then be written in the form

$$S(x) = S_K \left[\left(e^{V/V_a} + 1\right) \frac{\cos\left[k(x - L/2)\right]}{\cos kL/2} + \left(e^{V/V_a} - 1\right) \frac{\sin\left[k(x - L/2)\right]}{\sin kL/2} \right]. \tag{B16}$$

From Eqs. (B14), (B15), and (B16) we find

$$\cos\left(kL/2\right) = \frac{S_K}{2S_M} \left(e^{V/V_a} + 1\right) = \frac{e^{V_M/V_a}}{2} \left(e^{V/V_a} + 1\right) = \frac{S_K + S_A}{2S_M}. \tag{B17}$$

This equation constitutes a general dispersion relation for the wavenumber k.

We now consider the special case with no applied voltage $V = 0$. In this case the density values at the cathode and anode are equal, $S_K = S_A$, and Eq. (B17) reduces to

$$\cos\left(kL/2\right) = \frac{S_K}{S_M} = e^{V_M/V_a}. \tag{B18}$$

Note that a physical solution requires that V_M and V_a have the opposite sign, and that $S_K < S_M$, although we expect the density at the electrodes to be much smaller than in the middle of the plasma, $S_K \ll S_M$.

In Ref. [24], the diffusion equation is solved with the boundary condition $S_K = 0$. The wavenumber k is then obtained from $\cos\left(kL/2\right) = 0$. For the lowest order mode $kL = \pi$, or

$$\tau = \left(\frac{L}{\pi}\right)^2 \frac{1}{D_a}, \tag{B19}$$

with higher modes decaying away on time scales shorter than τ. We note that as $S_K/S_M \rightarrow 0$, the mid potential $V_M \rightarrow \infty$. This is clearly not physical, so some small but finite value of S_K/S_M should be retained. In this case, for the lowest order mode, $k < \pi/L$, which

corresponds to a longer time constant than predicted by Eq. (B19). When $V_a < 0$ (electrons are held back by the ambipolar field), the potential is concave down at $x = L/2$.

We consider somewhat more carefully here what happens when $S_K = 0$. In this case the density profile becomes

$$S(x) = S_M \cos\left[\pi(x/L - 1/2)\right]. \tag{B20}$$

We see from Eqs. (B1) and (B4), that this density profile leads to infinite fluid velocities at the cathode and anode surfaces. So near the walls, the diffusion approximation breaks down, *i.e.* it is no longer appropriate to neglect the convective derivative in the fluid momentum equations. From Eq. (B4), the ambipolar electric field also becomes infinite at the boundaries. However, the electric field is derived by arguing that quasi-neutrality justifies equating electron and ion fluxes. But quasi-neutrality is not maintained near the boundary surfaces. The scale-length for the non-neutral region is the plasma Debye length, so the treatment given in Ref. [24] gives a good estimate for the density profile when L is much larger than the Debye length. The actual physical value of V_M/V_a, however, depends on the details of the non-neutral sheath physics, and cannot be directly calculated from a quasi-neutral fluid theory.

We now consider the case of a non-zero applied voltage V. From Eq. (B16), the plasma center-of-mass may be calculated to be

$$\frac{\langle x - L/2 \rangle}{L} = \frac{1}{2}\left(\frac{e^{V/V_a} - 1}{e^{V/V_a} + 1}\right)\left(\frac{\cos(\alpha)}{\sin^2(\alpha)}\right)\left(\frac{\sin(\alpha)}{\alpha} - \cos(\alpha)\right), \tag{B21}$$

where $\alpha = kL/2$. Note that in the absence of an applied voltage, $V/V_a \to 0$, the plasma center-of-mass is exactly in between the two plates, $\langle x \rangle = L/2$. For a finite voltage V the center-of-mass may shift from the center. Determining the magnitude of the shift, however,

requires solving the dispersion relation for α. From Eq. (B17), this requires knowledge of the two parameters V/V_a and V_M/V_a. For the baseline simulation parameters given in Table I, $V = 100$ V, and $V_a \sim -5$ V, for which $e^{V/V_a} \ll 1$. In this limit, the first quantity in parenthesis on the right hand side of Eq. (B21) is approximately equal to -1, and the dispersion relation becomes

$$\cos(\alpha) \simeq \frac{e^{V_M/V_a}}{2}. \tag{B22}$$

As mentioned above, the value of the mid potential V_M cannot be determined by quasi-neutral fluid theory, but depends on the details of the sheath physics. Note that in contrast to the case with $V = 0$, a physical solution does not require $V_M/V_a < 0$. In this case it sufficient that $e^{V_M/V_a} < 2$. As V_M/V_a is decreased from its theoretical maximum of $+\ln(2)$, $\langle x - L/2\rangle/L$ increases monotonically from -0.25, to its asymptotic value of zero for $V_M/V_a \ll -1$, while α increases monotonically from zero to $\pi/2$.

If we estimate that $V_M/V_a \sim -1$ ($S_K/S_M \sim 0.37$), we obtain $\alpha \sim 1.39$, and

$$\frac{\langle x - L/2\rangle}{L} \sim -0.05, \tag{B23}$$

that is, the ion center of mass shifts by 5% towards the cathode. Suppose that for different values of electron and ion temperatures and collision frequencies, it occurs that $V_a > 0$, but that the magnitude of V_a is still much less than V, In this case, the first quantity in parenthesis on the right hand side of Eq. (B21) switches from ~ -1 to $\sim +1$. If we still assume that $V_M/V_a \sim -1$, then the center-of-mass shifts towards the anode side by 5%, instead of the cathode side. This demonstrates how the relative signs of V and V_a determine the direction of plasma shift. In fact, we can state the following general rule: when V_a is negative (electrons more mobile than ions), the density distribution will skew towards the

cathode. When V_a is positive (ions more mobile), the distribution skews towards the anode. This is regardless of the actual value of V_M (provided that it produces a physical result). The magnitude of the shift in center-of-mass does of course depend on V_M.

This theory predicts that for times $t \sim \tau$, after all higher-order modes have decayed away, $\langle x \rangle$ should be independent of time [a consequence of the ansatz in Eq. (B9)]. This is in contrast to the simulation results which show $\langle x \rangle$ decreasing monotonically with time, even for $t > \tau$. We must recall that this theory neglects important plasma transport phenomena. For example, the assumption of isothermal plasmas neglects Ohmic heating. Since Ohmic heating scales as the square of the electric field, we expect heating of the plasma species to be greater nearer the electrode where the ambipolar fields are largest. This will introduce a temperature profile which is not spatially uniform, which violates one of the key assumptions used to derive the simple diffusion equation. In effect, the temperature gradient will cause variations in the diffusion coefficient. Nonetheless, this theory does give a qualitative (and semi-quantitative) description of the simulation results presented in this report.

---

[1] E. F. Dirsa, Proc. IRE **48**, 703 (1960).

[2] R. Caldecott, P. Bohley, and J. W. Mayhan, IEEE Trans. Antennas Propagation **AP-17**, 786 (1969).

[3] J. P. Rybak and R. J. Churchill, IEEE Trans. Aerospace Electronic Systems **AES-7**, 879 (1971).

[4] N. D. Akey and A. E. Cross, *Radio blackout alleviation and plasma diagnostic results from a 25,000 foot per second blunt-body reentry*, NASA Technical Note, No. TN-5615, 1970.

[5] P. Huber, *The entry plasma sheath and its effects on space vehicle electromagnetic systems*,

NASA Technical Note, No. SP-252, 1971.

[6] R. P. Starkey, *Electromagnetic wave/magnetosctive plasma sheath interaction for hypersonic vehicle telemetry blackout analysis*, Proceedings of the 34th AIAA Plasmadynamics and Lasers Conf. June 23-26, 2003, Orlando, FL.

[7] R. P. Starkey, *Nonequilibrium plasma effects on telemetry considerations for air-breathing hypersonic vehicle design*, Proceedings of the 42th AIAA Aerospace Sciences Meeting and Exhibit, January 5-8, 2004, Reno, NV.

[8] D. V. Rose, T. C. Genoni, T. P. Hughes, R. E. Clark, C. Thoma, D. R. Welch, and V. Sotnikov, *Analysis of plasma communication schemes for hypersonic vehicles: progress report 3*, Voss Scientific Report No. VSL-0737, November 15, 2007.

[9] S. V. Nazarenko, A. C. Newell, and V. E. Zakharov, Phys. Plasmas **1**, 2827 (1994).

[10] S. V. Nazarenko, A. C. Newell, and A. M. Rubenchik, Radio Sci. **30**, 1753 (1995).

[11] A. O. Korotkevich, A. C. Newell, and V. E. Zakharov, J. Appl. Phys. **102**, 083305 (2007).

[12] C. Thoma, T. P. Hughes, and D. V. Rose, *Theory and simulation results on the plasma sheath magnetic window*, Voss Scientific Report No. VSL-0738, December 2007.

[13] V. I. Sotnikov, M. Ashour-Abdalla, D. Schriver, and V. Fiala, Radio Sci. **28**, 1087 (1993).

[14] V. I. Sotnikov, D. Schriver, M. Ashour-Abdalla, and J. Ernstmeyer, J. Geophys. Res. **A99**, 8917 (1994).

[15] D. Schriver, V. I. Sotnikov, M. Ashour-Abdalla, and J. Ernstmeyer, J. Geophys. Res. **A100**, 3693 (1995).

[16] LSP is a software product developed by ATK Mission Research, Albuquerque, NM 87110, with initial support from the Department of Energy SBIR Program.

[17] D. Morris, M. Keidar, and I. Boyd, *Recomm - reentry and hypersonic vehicle plasma commu-*

nication, Presented at the Workshop on Communications Through Plasma During Hypersonic Flight.

[18] M. Keidar, M. Kim, and I. D. Boyd, J. Spacecraft and Rockets **45**, 445 (2008).

[19] G. S. Janes and R. S. Lowder, Phys. Fluids **9**, 1115 (1966).

[20] C. Thoma, T. P. Hughes, N. L. Bruner, T. C. Genoni, D. R. welch, and R. E. Clark, IEEE Trans. Plasma Sci. **34**, 910 (2006).

[21] C. Thoma, D. R. Welch, D. V. Rose, L. K. Warne, and R. E. Jorgenson, *Computational modeling of high pressure gas breakdown and streamer formation in external electric fields*, Voss Scientific Report, No. VSL-0621, September 2006.

[22] D. V. Rose, D. R. Welch, C. Thoma, L. K. Warne, and R. E. Jorgenson, *Computational modeling of high pressure gas breakdown and streamer formation in external electric fields*, proc. of the 2007 IEEE Pulsed Power and Plasma Science Conf. 2007, E. Schamiloglu and F. Peterkin, editors, p. 1205.

[23] D. R. Welch, C. Thoma, and R. E. Clark, *8^{th} quarterly report: Testing of the new sheath model on the Hyper-V accelerator*, Voss Scientific Report, No. VSL-0811, May 2008.

[24] F. F. Chen, *An Introduction To Plasma Physics and Controlled Fusion* (Plenum Press, New York, 1984).

[25] N. E. Andreev and A. Y. Kirii, Sov. Phys. Tech. Phys. **16**, 854 (1971).

[26] M. Porkolab, Phys. Fluids **17**, 1432 (1974).

[27] G. Bonizzoni, M. Fontanesi, G. Grosso, E. Lazzaro, and E. Sindoni, Plasma Phys. **19**, 1163 (1977).

[28] M. Kim, M. Keidar, and I. D. Boyd, J. Spacecraft and Rockets **45**, 1223 (2008).

[29] M. Kim, M. Keidar, and I. D. Boyd, IEEE Trans. Plasma Sci. **36**, 1198 (2008).

[30] H. Hodara, Proc. IRE **49**, 1825 (1961).

[31] M. J. Nusca, J. Thermophys. Heat Transfer **11**, 304 (1997).

[32] M. J. Nusca, Computers and Fluids **27**, 217 (1998).

[33] E. Josyula and W. F. Bailey, J. Spacecraft and Rockets **40**, 845 (2003).